Int. J. Electrochem. Sci., 7 **(2012)** 2710 - 2763

International Journal of
ELECTROCHEMICAL
SCIENCE
www.electrochemsci.org

Redox Switching and Oxygen Evolution at Hydrous Oxyhydroxide Modified Nickel Electrodes in Aqueous Alkaline Solution: Effect of Hydrous Oxide Thickness and Base Concentration

Michael E.G. Lyons[*], *Lisa Russell, Maria O'Brien, Richard L. Doyle, Ian Godwin, Michael P Brandon*

Trinity Electrochemical Energy Conversion and Electrocatalysis (TEECE) Group, Physical and Materials Electrochemistry Laboratory, School of Chemistry, University of Dublin, Trinity College, Dublin 2, Ireland.
[*]E-mail: melyons@tcd.ie

Received: 8 December 2011 / *Accepted:* 28 February 2012 / *Published:* 1 April 2012

Outstanding issues regarding the film formation, the redox switching reaction and the oxygen evolution reaction (OER) electrocatalytic behaviour of multi-cycled nickel oxy-hydroxide films in aqueous alkaline solution have been discussed. The oxide is grown using a repetitive potential multi-cycling technique, and the mechanism of the latter hydrous oxide formation process has been discussed. A duplex layer model of the oxide/solution interphase region is proposed. The acid/base behaviour of the hydrous oxide and the microdispersed nature of the latter material has been emphasized. The hydrous oxide is considered as a porous assembly of interlinked octahedrally coordinated anionic metal oxyhydroxide surfaquo complexes which form an open network structure. The latter contains considerable quantities of water molecules which facilitate hydroxide ion discharge at the metal site during active oxygen evolution, and also charge compensating cations. The dynamics of redox switching has been quantified in terms of a diffusive frequency via analysis of the cyclic voltammetry response as a function of potential sweep rate using the Laviron-Aoki electron hopping diffusion model by analogy with redox polymer modified electrodes. Potential step chronoamperometry applied to hydrous oxide coated Ni surfaces has indicated that the Ni(II)/Ni(III) redox switching reaction is quite complex. Steady state Tafel plot analysis has been used to elucidate the kinetics and mechanism of oxygen evolution. Tafel slope values of ca. 60 $mVdec^{-1}$ and ca. 120 $mVdec^{-1}$ are found at low and high overpotentials respectively, whereas the reaction order with respect to hydroxide ion activity remains invariant at ca. 1.0 as the potential is increased. These observations are rationalized in terms of a kinetic scheme involving Langmuir adsorption and the formation of a physisorbed hydrogen peroxide intermediate on the oxide surface. The dual Tafel slope behaviour is ascribed to the changeover in rate determining step from the second chemical hydroxide ion reorganization step to the first initial discharge step as the potential is increased, which is in contrast to the potential dependence of the surface coverage of adsorbed intermediates which holds for hydrous iron oxide electrodes in base.

Keywords: oxygen evolution electrocatalysis, oxidized nickel electrodes, hydrous oxide modified electrodes, oxygen evolution mechanisms

1. INTRODUCTION

The oxygen evolution reaction (OER) is the anodic reaction that accompanies, in aqueous electrolytes, commerically important cathodic processes such as metal electrowinning and hydrogen production via alkaline water electrolysis. For the latter process, the anodic overpotential is the major factor in limting operational efficiency [1]. The optimal oxygen evolution anode materials are RuO_2 and IrO_2, since these oxides exhibit the lowest overpotentials for the reaction at practical current densities. The high cost of these materials and their poor long term stability in alkaline solution, renders their widespread commercial utilisation both uneconomical and impractical [2]. Nickel and its alloys have therefore become the anodes of choice for water electrolysis [1,2]. Although the OER overpotential is higher than for RuO_2 or IrO_2, nickel based electrodes are relatively inexpensive and display excellent corrosion resistance in aqueous alkaline media, and thus offer an attractive compromise solution. That said, the OER electrocatalytic performance of metallic Ni (actually passive oxide covered Ni) in alkaline solution diminishes markedly with time [3].

In view of the latter considerations, there has been, over the past thirty years, extensive research focussed on the development of OER electrocatalysts that display a combination of the desired characteristics of long term physical and chemical stability, satisfactorily low reaction overpotential and viable cost. Amongst the most promising materials that have been forwarded as OER anodes are, various inter-metallic alloys (often containing significant amounts of Ni, Co or Fe), electrodeposited Ni (NiO_x) and Co (Co_3O_4) oxides, and mixed oxides, including spinels(particularly nickelites, cobaltites and ferrites) and perovskites. While the relatively high activity of nickel hydroxide electrodes for the OER is welcome in alkaline electrolyser applications, it is a drawback where this material is utilised as the positive electrode in secondary alkaline batteries (e.g. Ni-Cd, Ni-MH and Ni-MH_2) since it facilitates "self discharge" and consequently leads to a decrease of charge storage capacity [4,5]. Thus in contrast to electrolyser anode research, work in the battery area has been directed towards increasing the OER overpotential at nickel hydroxide electrodes. This has been achieved by the addition of cobalt hydroxide to the nickel hydroxide [6], however, depending on the amount of incorporated Co, this procedure can actually improve OER catalytic activity [7]. These oxides have been prepared from inorganic precursor materials using a wide variety of approaches, including thermal decomposition, spray pyrolysis, sol-gel routes and freeze drying, precipitation or electrodeposition from solution.

Despite all this intense activity the mechanism of the OER at first row transition metal oxide surfaces remains controversial. The experimental confirmation that a common OER mechanism pertains for these materials would be a significant aid in the eventual development of a general predictive theory of OER electrocatalysis for such materials.

In the present paper we examine the mechanism both of redox switching and anodic oxygen

evolution at oxidized nickel electrodes in alkaline solution using a combination of steady state polarization techniques and reaction order studies. We propose a mechanism for the latter which specifically takes the nature of the electrochemically generated hydrous oxide film that is present on the surface of the Ni electrode during active oxygen evolution into account. This work follows on from our recently published studies on the interfacial redox chemistry, redox switching mechanism and OER electrocatalytic activity of oxidized transition metal electrodes [8-10] and iron electrodes modified with microdispersed hydrous oxy hydroxide films [11-16].

2. EXPERIMENTAL

All experiments were conducted in a conventional three electrode cell. The working electrode was constructed from 1mm thick polycrystalline nickel foil (as supplied by Alfa Aesar-Johnson Matthey, purity 99.9945% (metals basis)) with a geometric surface area of 0.16 cm^2. Prior to each experiment the surface of the working electrode was polished with 1200 grit carbimet paper, dipped in H_2SO_4, wiped, and polished with a slurry of 0.3 micron alumina powder until a "mirror bright" finish was achieved. A platinum wire electrode (CH Instruments, cat no. CHI 115) was employed as the counter electrode and a mercury-mercuric oxide (Hg/HgO) reference electrode (CH Instruments, cat no. CHI 152) was utilised as the reference standard, therefore all voltages are quoted against this reference electrode[1]. When used in NaOH solutions of different concentrations, the potential of the Hg/HgO electrode was checked relative to a second Hg/HgO, 1 M NaOH electode, both before and after the experiment. No significant potential drift was noted after such experiments, implying that the concentration of the NaOH in the reference electrode chamber remains effectively constant over the time scale of typical polarisation measurements. In any case, the 1M NaOH solution in the reference electrode, was changed regularly to ensure experimental consistency.

Aqueous NaOH solutions (in the range between 0.1 and 5.0 M) served as both the electro-polymerisation medium and the supporting electrolyte for the redox switching and electrocatalytic studies. This solution was prepared from sodium hydroxide pellets (Sigma-Aldrich, minimum 99% purity) using Millipore water (resistivity > 15 MΩ cm). Before commencing each experiment, nitrogen gas was bubbled through the electrolyte solution for 20 min.

The electrochemical measurements were performed using a number of high performance digital potentiostats including a BAS 100B Electrochemical Analyser and a CH Model 760 D Bi-potentiostat system.

Both workstations were controlled by high end desktop Personal Computers (Dell). The uncompensated solution resistance was determined using a method developed by He and Faulkner [17]. Typically the uncompensated solution resistance (90% compensation level) varies from ca. 0.30

[1] The equilibrium potential of the cell $Pt/H_2/OH^-/HgO/Hg$ is 0.926 V at 298 K. Since the equilibrium oxygen electrode potential is 1.229 V vs RHE, it follows that the corresponding value is 0.303 V vs Hg/HgO in the same solution. Hence $E_{Hg/HgO} = E_{RHE} - 0.926$ V. It is common practice in the literature on the OER to express potential in terms of the oxygen overpotential η, when the reference electrode is a Hg/HgO electrode in the same solution as the working anode. Clearly, in this case the overpotential η is related to E_{meas} measured on the Hg/HgO scale as follows: $\eta = E_{meas} - 0.303$ V (at T = 298 K).

Ω for $[OH^-]$ = 5.0 M to ca. 4.3 Ω for $[OH^-]$ = 0.1 M. This parameter was specifically considered in the Tafel plot measurements, where the data is presented in *iR* compensated form. Unless otherwise specified, all values of current density are normalised with respect to the geometric surface area.

Charge storage capacity (redox capacity), *Q*, were determined via integration of the peaks recorded in the voltammetric profiles at slow sweep rates. The redox capacity is directly proportional to the layer thickness.

The polymeric Ni oxy-hydroxide films were prepared *via* multi-cycling the Ni electrode between the switching potentials of -1.450 V and 0.65 V at a scan rate of 0.15 V s^{-1}. Films of different thicknesses were prepared by varying the number of growth cycles. The charge storage capacity or redox capacity (Q) was determined, following the growth of each film, by integration of the peaks in a voltammetric profile recorded at a slow sweep rate (40 mV s^{-1}). The redox capacity is directly proportional to the layer thickness. Tafel plots were recorded for each film using linear sweep voltammetry performed at a sweep rate of 1 mV s^{-1}.

3. RESULTS AND DISCUSSION

3.1 Hydrous Oxide growth via repetitive potential sweep multicycling (RPSM)

As commented by Gottesfeld and Srinivasan; " the "science" of the OER is a "science" of the oxides and their properties" [18]. We agree that this statement is particularly pertinent for Ni electrochemistry in base. One of the most versatile and convenient techniques used to generate hydrous oxides in a form suitable for the real time determination of their redox switching and electrocatalytic behavior is that of potential cycling . In this method the potential of an electrode of the parent metal (which may be noble or non-noble) is cycled repetitively between suitable lower and upper limits in an aqueous solution of appropriate pH. The type of potential perturbation used for oxide growth – sinusoidal, square or triangular wave- apparently makes little difference . Indeed the triangular wave is most convenient as changes in the current vs potential response (the voltammogram) can be employed during the oxide growth reaction to monitor changes in redox behavior associated with the latter [22], although Arvia and co-workers [23] contend that a repetitive square wave potential pulse is also very effective for the controlled generation of hydrated metal oxy-hydroxide films on metallic supports, especially if one wishes to form relatively thick oxide films. Typical voltammetric profiles recorded for an initially bright, and multicycled Ni electrodes in 1.0 M NaOH are presented in figures 1 – 3. The sweep rate utilized was 50 mV/s.

These voltammograms are similar in shape to those previously reported in the literature, most notably by Burke and co-workers [24], Visscher and Barendrecht [25], de Souza et al. [26] and Simpraga and Conway [27] to name but a few.

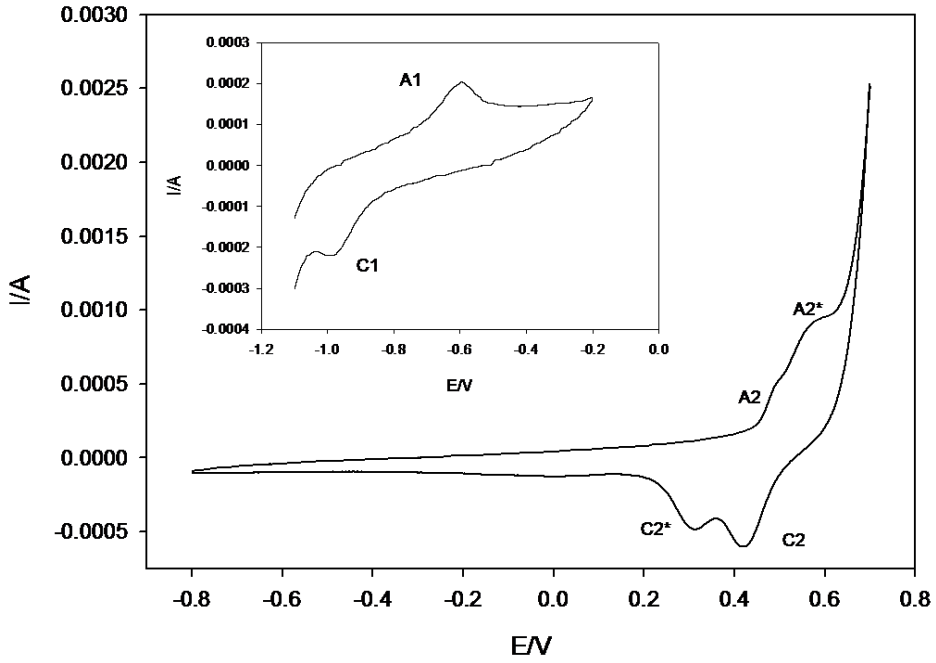

Figure 1. Typical cyclic voltammetric response recorded for an uncycled Ni electrode in 1.0 M NaOH. Sweep rate, 50 mV/s. Inset shows the peak set labeled A_1 and C_1 recorded at low potentials prior to the onset of active hydrogen evolution at ca. – 1.08 V (vs Hg/HgO).

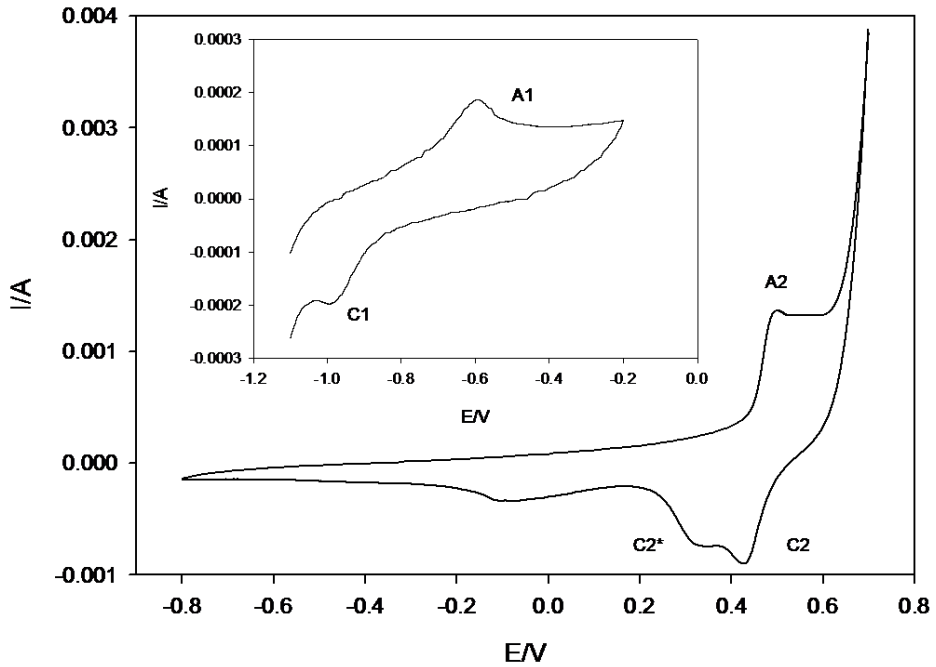

Figure 2. Typical cyclic voltammetric response recorded for multi-cycled (N = 30 cycles) Ni electrode in 1.0 M NaOH. Sweep rate, 50 mV/s. Inset shows the peak set labeled A_1 and C_1 recorded at low potentials prior to the onset of active hydrogen evolution at ca. – 1.08 V (vs Hg/HgO).

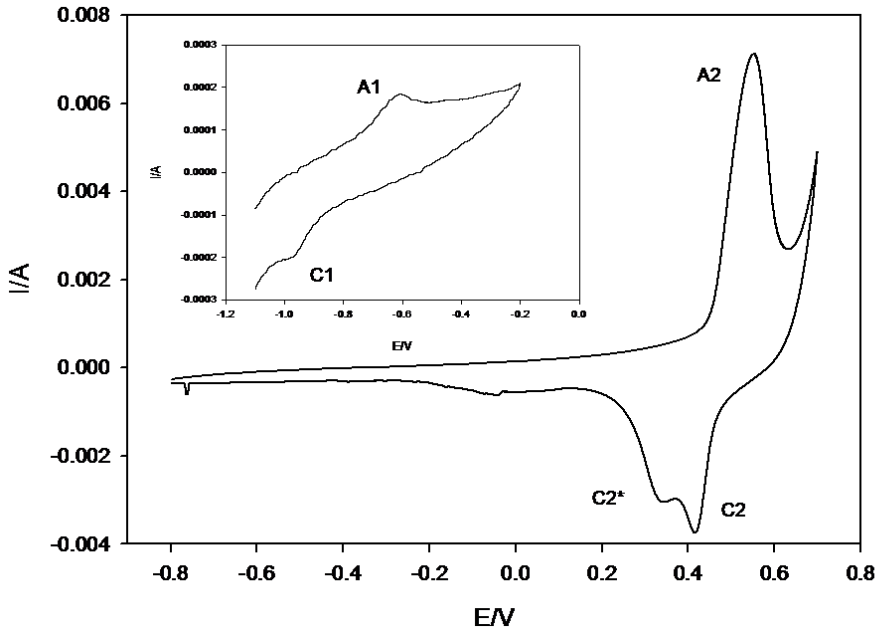

Figure 3. Typical cyclic voltammetric response recorded for multi-cycled (N = 300 cycles) Ni electrode in 1.0 M NaOH. Sweep rate, 50 mV/s. Inset shows the peak set labeled A_1 and C_1 recorded at low potentials prior to the onset of active hydrogen evolution at ca. – 1.08 V (vs Hg/HgO).

It is almost universally agreed that the lower anodic peak observed in the potential region between -0.6 V and – 0.8 V is principally associated with the oxidation of metallic Ni(0) to Ni(II) species. There has been historically some disagreement about the nature of the Ni(II) oxide species formed at this potential with, for example, Makrides[28] proposing the production of NiO and $Ni(OH)_2$, while Okuyama [29] suggested that the oxide film in this potential region was non-stoichiometric, consisting of NiO and Ni_3O_4. By analogy with the situation found at low potentials for Fe in base [15,16] we can visualize the following sequence of reactions at low potentials:

$$Ni + OH^- \rightarrow NiOH_{(ads.)} + e^- \quad (1)$$

$$NiOH_{(ads.)} + OH^- \rightarrow Ni(OH)_2 + e^- \quad (2)$$

$$NiOH_{(ads.)} + OH^- \rightarrow NiO_{(ads)} + H_2O + e^- \quad (3)$$

The overall interfacial reaction resulting in Fe(II) film formation may be more complex than that outlined above due to a variety of other possible reactions. For instance hydroxylation reactions such as:

$$NiO + H_2O \rightarrow Ni(OH)_2 \quad (4)$$

will result in the conversion of oxy to hydroxy species in the outer region of the surface

layer. Place exchange processes [30] can result in an increase in the thickness of the surface layer. The latter type of growth process has been proposed to involve a rapid place exchange step followed by a rate determining Temkin discharge of OH^- ions onto sites in which a surface iron atom is already attached to a hydroxyl group displaced into the first layer beneath the surface, viz:

$$NiOH_{(ads)} \rightarrow HONi \quad \text{(fast)} \tag{5}$$

$$HONi + OH^- \rightarrow HONiOH_{(ads)} \quad \text{(slow rds)} \tag{6}$$

$$HONiOH_{(ads)} \rightarrow Ni(OH)_2 \rightarrow NiO + H_2O \tag{7}$$

One should note that with a non noble metal such as Nickel or iron, the aforementioned surface processes are likely to be accompanied by film thickening (i.e. place exchange reactions [30]), even at quite low potentials.

More recently the complex nature of the film even at these low potentials has been emphasised. Based on the variation of the voltammetric peak potential with changes in pH in alkaline solution (typically the redox potential for the anodic reaction decreases by ca. 13 mV per unit change in pH with respect to a pH independent reference electrode), Burke and Twomey [24] proposed that both oxidation and hydrolysis processes were operative in this region, leading to the formation of a species with anionic character which was tentatively assigned, for purposes of rationalization, the formula $Ni(OH)_{2.4}^{0.4-}$. The reaction sequence proposed by the latter workers was:

$$Ni + 2\ OH^- \rightarrow Ni(OH)_2 + 2\ e^- \tag{8}$$

$$Ni(OH)_2 \rightarrow [NiO_{0.4}(OH)_{1.6}]^{0.4-} + 0.4\ H^+ \tag{9}$$

Note that eqn.9 may be represented as a hydroxide ion adsorption step since the reaction occurs in alkaline solution:

$$Ni(OH)_2 + 0.4\ OH^- \rightarrow Ni(OH)_{2.4}^{0.4-} \tag{10}$$

Hence in very simple terms the net anodic reaction corresponding to peak A_1 can be represented as:

$$Ni + 2.4\ OH^- \rightarrow [Ni(OH)_{2.4}]^{0.4-} \tag{11}$$

When the anodic limit of the potential sweep was maintained well below the upper redox charge storage peaks, Burke and Twomey [24] observed a pH invariant cathodic peak at potentials some 0.3 V lower than the anodic peak. It is clear from fig.1 – fig. 3 that similar results have been found in the present studies. A distinct pair of peaks (A_1 and C_1) are present at low potentials in

the region – 0.6 to -1.0 V (vs Hg/HgO) irregardless of whether the nickel electrode has been subjected to a potential multicycling perturbation or not. The cathodic peak C_1 is observed provided the upper limit of the potential sweep is reversed at a potential (ca. – 0.2 V) far from the onset of the development of the main charge storage peaks (the latter occur at E > 0.2 V). We agree with the conclusion proposed by Burke and Twomey [24] that the reversal in sweep direction at low potentials causes the initially produced hydrous oxide species to transform to a more anhydrous form, such as to NiO say. Hence the C_1 reduction peak could be due to:

$$NiO + H_2O + 2e^- \rightarrow Ni + 2\ OH^- \quad (12)$$

In essence the Burke-Twomey [24] proposal is that due to post electrochemical place exchange reactions, the anionic oxide becomes neutral before being reduced back to Ni metal. They also suggest that that the lower oxidation peak appears to be superimposed on a background current that is probably due to a combination of adsorbed hydrogen oxidation and formation of a layer of adsorbed hydroxyl species as outlined in eqn.1. In an ellipsometric study de Souza et al.[26] found that the first layer of oxide formed at potentials close to the lower anodic peak A_1 consists of NiO. However this becomes covered with a thick film of $Ni(OH)_2$ upon further increase of potential. A further significant observation of Burke and Twomey [24] was that the magnitude and position of the lower anodic peak did not alter much with repetitive potential cycling. Our data presented in fig. 1 – fig. 3 support this observation. We therefore support the Burke-Twomey [24] contention that it is the inner, compact oxide layer that is reduced at significant cathodic potentials, and thus, even on cycling, the A_1 peak is associated with oxidation of Ni metal to Ni(II) at the metal/porous hydrous oxide interface.

Two distinct sets of anodic (A_2, A_2*) and cathodic (C_2, C_2*) peaks may be observed at more elevated anodic potentials greater than ca. 0.20 V at a Ni electrode that has not been subjected to a multicycling procedure (fig.1). Peak A_2* disappears on potential multicycling and peak A_2 increases considerably in magnitude with increasing number of potential cycles as noted in fig. 2 for N = 30 cycles, and in fig.3 for N = 300 cycles. The cathodic peak doublet C_2 and C_2* remain even after considerable multicycling corresponding to the formation of a thick hydrous oxide deposit on the nickel surface. Hence raising the upper limit of the voltammetric sweep from – 0.20V to E > 0.7 V ensures the occurrance of further restructuring of the surface layer involving more complete protonation and further uptake of oxygen resulting not only in increased film thickness but also generation of Ni(III) or even Ni(IV) sites in the oxide film. This results in the generation of a more stable oxide coating so that the lower cathodic peak C_1 at – 0.95 V is no longer observed (fig. 2 and fig. 3). The lower limit of the potential sweep has to be extended well into the active hydrogen evolution region before significant reduction of the hydrous oxide occurs. Indeed we have found that the optimum lower limit for efficient hydrous oxide formation is ca. – 1.45 V.

We have previously noted that even though it is directly produced in the initial electrochemical oxidation process, the anhydrous film is probably not the most stable metal oxidation product in the aqueous medium but it may be regarded as an intermediate or metastable

product in the formation of a hydrous oxide layer. In the anhydrous film ions are held in a rigid manner in an extended network of polar covalent bonds which drastically reduce ion transport through (and consequently extension of) the surface layer. The next stage of the film thickening process, the hydration reaction, is generally very slow, because as in phase transformation reactions, it involves rupture of primary coordination metal-oxygen bonds. It has been shown that the extent of hydrous oxide growth depends strongly on the value chosen for the upper and lower limit of the potential sweep as well as on the cycling frequency adopted, the solution temperature and the solution pH.

The marked dependence of oxide growth rate on the lower limit of the potential sweep (found for a wide number of noble and non-noble transition metals) is indicative of the essential role that partial reduction of the anhydrous oxide plays in the production of a thick deposit. Partial reduction of the compact oxide layer apparently facilitates rearrangement of oxycation species at the metal surface, leaving it in a somewhat disrupted state. It is established that in the case of both platinum [32] and gold [32, 33] the anhydrous film is reduced much more readily than the hydrated film. The greater stability of the latter is possibly due to a variety of reasons such as lower repulsion between cations owing to greater separation and decreased charge (the latter effect being due to hydroxyl ion coordination by cations present) and polymer formation. Indeed it has been established that in the case of metal-gas interactions [34] the adsorption-desorption process effects displacement of atoms in the outer layer of the metallic phase, and that potential cycling causes roughening of the surface of noble metals such as platinum under certain conditions [35].

On subsequent re-oxidation of the partially reduced metal surface the compact layer is restored but the outer region of the compact film is present in a more dispersed form. On further reduction the latter material becomes incorporated into the hydrated outer layer. It is not clear whether this rearrangement process involves detachment of oxycations, i.e. a dissolution-reprecipitation mechanism, or a certain weakening, with only a partial detachment of oxycation binding in the compact oxide layer. In the latter case the partially reduced cations are assumed to be displaced from normal lattice sites, and, as such, are more susceptible to oxidation in the subsequent anodic sweep during which they complete their oxygen coordination shell of six oxygen atoms to form a rather open polymeric inorganic bronze or zeolite type structure. Hence under conditions of thick film growth the interfacial region may be represented by : $M/MO_x/MO_a(OH)_b(OH_2)_c$/aqueous phase as is outlined in figure 4. This is the duplex layer model of the oxide/solution interphase region. Here MO_x represents the inner compact layer and $MO_a(OH)_b(OH_2)_c$ denotes the outer hydrous layer. This model was first suggested by Burke and O'Sullivan [36].

Hence the appearence of the lower anodic peak A_1 and the enhanced hydrous oxide growth reaction (see figure 5 for example) only occur under potential cycling conditions when the lower limit of the potential sweep is set at a magnitude sufficiently cathodic to ensure extensive reduction at the compact/support electrode interface.

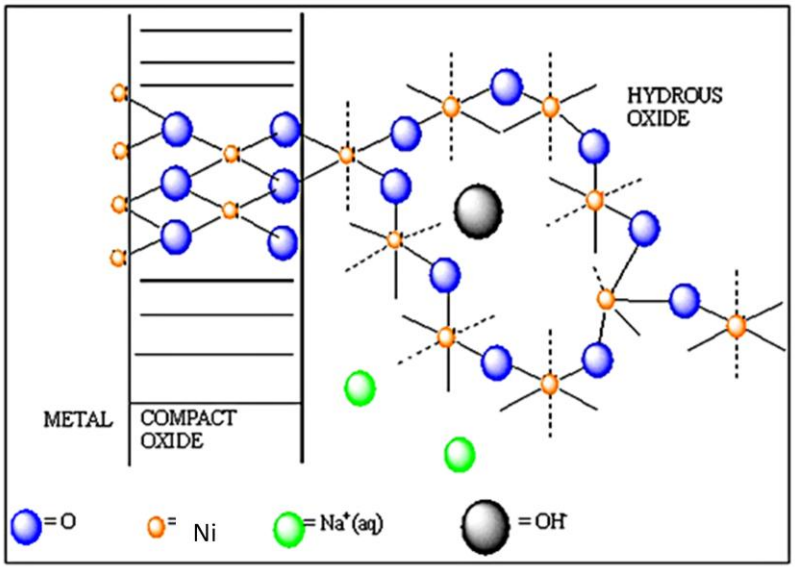

Figure 4. Burke-O'Sullivan [36] duplex layer model of oxide/solution interface.

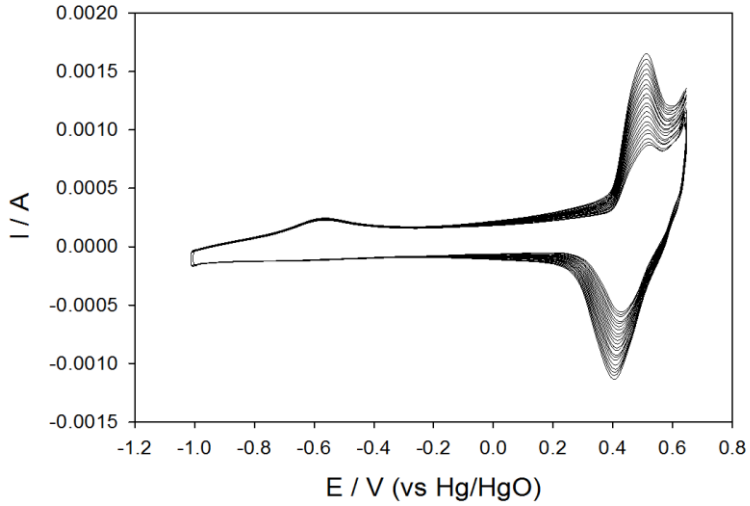

Figure 5. Growth of hydrous nickel oxide thin film on Ni support electrode monitored via analysis of the evolution of the real time voltammogram in 1.0 M NaOH. Sweep rate 350 mV/s.

The upper peaks observed in the potential region 0.3 to 0.6 V are greatly enhanced when the Ni support electrode is subjected to a repetitive potential sweep. These are labeled the main charge storage or redox switching peaks. However only peak A_2 and the cathodic doublet peaks C_2 and C_2* may be observed when the electrode surface is coated with a thick hydrous oxide layer.

The interfacial redox chemistry of the multicycled nickel oxide electrode in aqueous alkaline solution can be readily understood in terms of the Bode scheme of squares [37]. Here the redox switching behaviour of electrochemically generated nickel oxide films was rationalized in terms of four phases as outlined in fig.6 below.

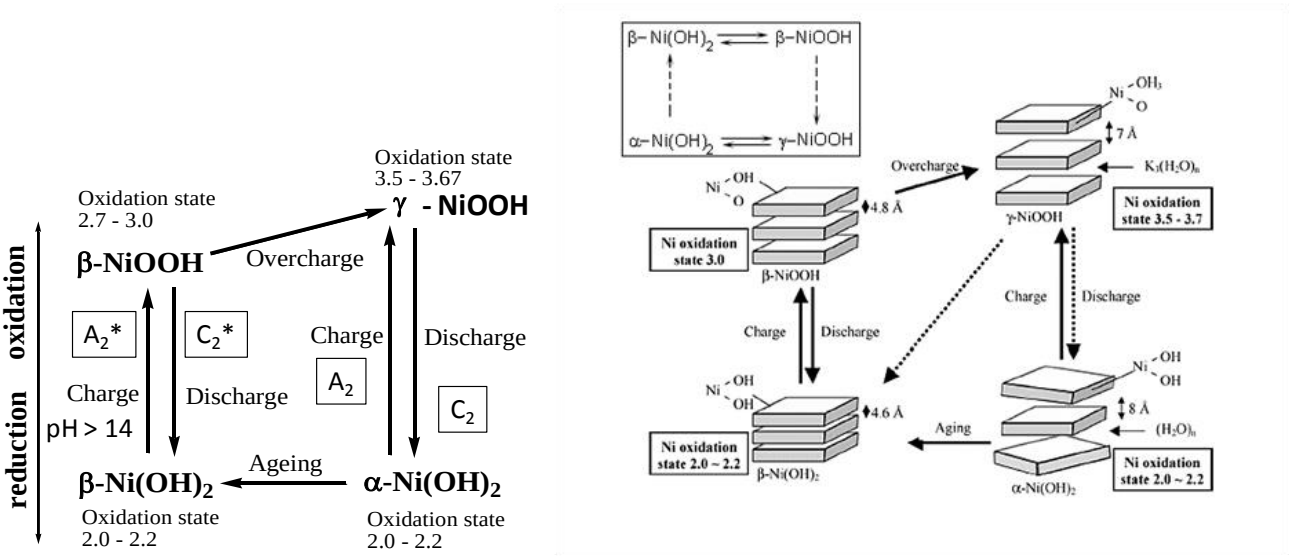

Figure 6. Schematic representation of Bode Scheme of squares.

The discharged or reduced $Ni(OH)_2$ material can exist either as a largely anhydrous phase designated as β – $Ni(OH)_2$ (denoted β-Ni(II)) or as a hydrated phase denoted as α-$Ni(OH)_2$ (in short represented as α-Ni(II)). Oxidation of the β-Ni(II) material is envisaged to produce a phase referred to as β-NiOOH or β-Ni(III). In contrast oxidation of the α-Ni(II) material produces γ-Ni(III) or γ-NiOOH. Hence one expects two distinct redox transitions : β(II)/β(III) and α(II)/γ(III). The corresponding redox peaks are designated A_2*/C_2* and A_2/C_2 respectively. Burke and Twomey designated the latter peak sets as A_A/C_A and A_H/C_H respectively. We note from fig.6 that upon ageing, especially in more concentrated alkali solution, the α-$Ni(OH)_2$ can dehydrate and re-crystallize as β-$Ni(OH)_2$. Furthermore, upon overcharge (which occurs at more elevated potentials) β-NiOOH can convert to γ-NiOOH. The non-stoichiometric nature of both the discharged and charged material is indicated by the average oxidation state of Ni in each phase as indicated in the structural representation of the various phases in the rhs schematic presented in fig.6. It is important to note that while there is a general acceptance for the general features of the Bode scheme, one must understand that it is inappropriate to think about the formation of a compound or a phase with definite stoichiometry during the chemically complex $Ni(OH)_2$/NiOOH transformation. Instead the four phases mentioned in the Bode scheme should be considered as the limiting forms of the divalent and trivalent materials – the actual composition of the oxide at a given potential depending on a range of factors including its history, method of preparation, degree of hydration, defect concentration etc.

In simple terms peaks A_2*/C*$_2$, can be attributed to the following Ni(II)/Ni(III) redox transformation:

$$Ni(OH)_2 + OH^- \rightarrow NiOOH + H_2O + e^- \quad (13)$$

According to Burke and Lyons [38] the potential for an ideal oxide electrode system in aqueous solution at 25ºC, decreases with increasing pH by ca. 59 mV/pH unit, with respect to a pH independent reference electrode such as the NHE or the saturated calomel electrode (SCE). Such a shift in potential with pH, is referred to as a *Nernstian shift*, since it is predicted by the Nernst equation. It should be noted that if the reference electrode is pH dependent, such as the reversible hydrogen electrode (RHE) or the Hg/HgO electrode, no potential pH shift will be observed, since the potential of this type of electrode also alters by ca. 59 mV per unit change in pH at 25ºC. Furthermore, Burke and Lyons [38] have discussed super-Nernstian shifts that have been observed for various hydrous oxide systems – in these cases the potential/pH shift differs from the expected 0.059V/pH unit at 25^0C. The mathematical treatment of this situation is beyond the scope of the present review, but suffice to say, the phenomena have been qualitatively summarized [24,38,39]. Thus, a zero potential shift (with respect to a pH dependent reference electrode) implies that both the reactants and the product possess the same net charge. A positive potential shift with pH, is indicative of an oxidised state that is more positive than the reduced state, whereas the converse is true in the case of an observed negative potential/pH shift.

However, it was previously shown [24] that the anhydrous A_2*/C*$_2$ peaks exhibit a regular Nernstian shift whereas the hydrous counterparts A_2/C_2 exhibit the characteristic of a hydrous or hyper-extended oxide [38], i.e. *a super-nernstian potential-pH shift*, which typically has the value of dE/dpH = -2.303(3RT/2F) = -0.088V/pH unit at T = 298 K. Accordingly, by analogy with a scheme produced by Burke and Whelan [40] for redox switching of iridium oxide films, it has been proposed that the main redox switching reaction may be written as:

$$[Ni_2(OH)_6(OH_2)_3]_n^{2-} + 3nOH^- \rightarrow [Ni_2O_3(OH)_3(OH_2)_3]_n^{3-} + 3nH_2O + 2ne^- \quad (14)$$

corresponding to an Ni(II)/Ni(III) redox transition in a polymeric microdispersed hydrous oxide layer. This redox switching reaction is illustrated schematically in scheme A below.

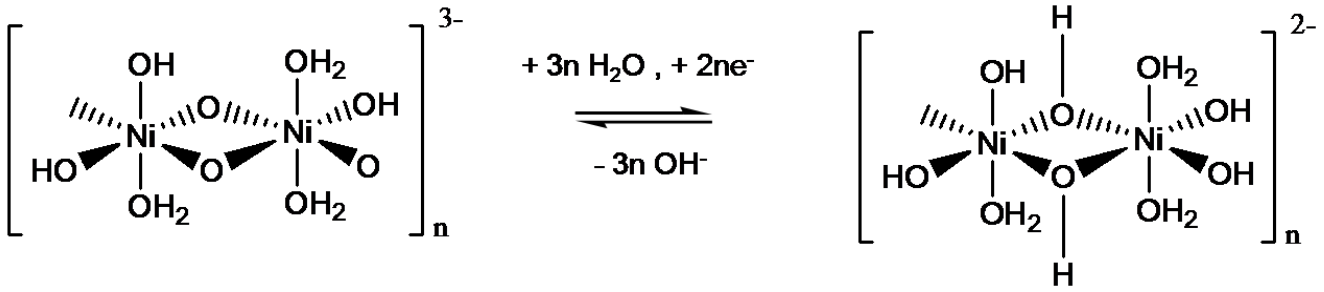

Scheme A

We have noted that the voltammetry exhibited by multicycled oxide coated Ni electrodes is strongly dependent on the concentration of base in which the oxide electrode is in contact with. In our experiments the Ni electrode was subjected to a potential multicycling procedure in 1.0 M NaOH for a fixed number of cycles in order to generate a thick oxide film. The latter film coated electrode was then cycled in a series of solutions of varying base concentrations in the range 0.1 to

5.0 M. Typical results are presented for moderate cycling (N = 30 cycles) in fig.7 and for more extended multicycling (N = 120) in fig. 8. Attention is focused on the Ni(II)/Ni(III) redox transition involving the peaks A_2, C_1* and C_2.

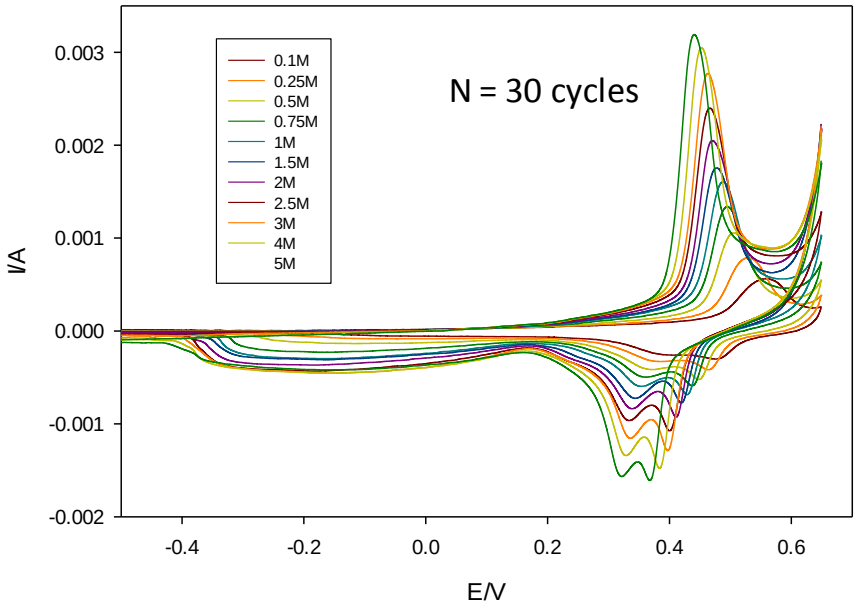

Figure 7. Voltammetric behaviour of a multicycled (in 1.0 M NaOH for N = 30 cycles) oxide coated Ni electrode as a function of base concentration.

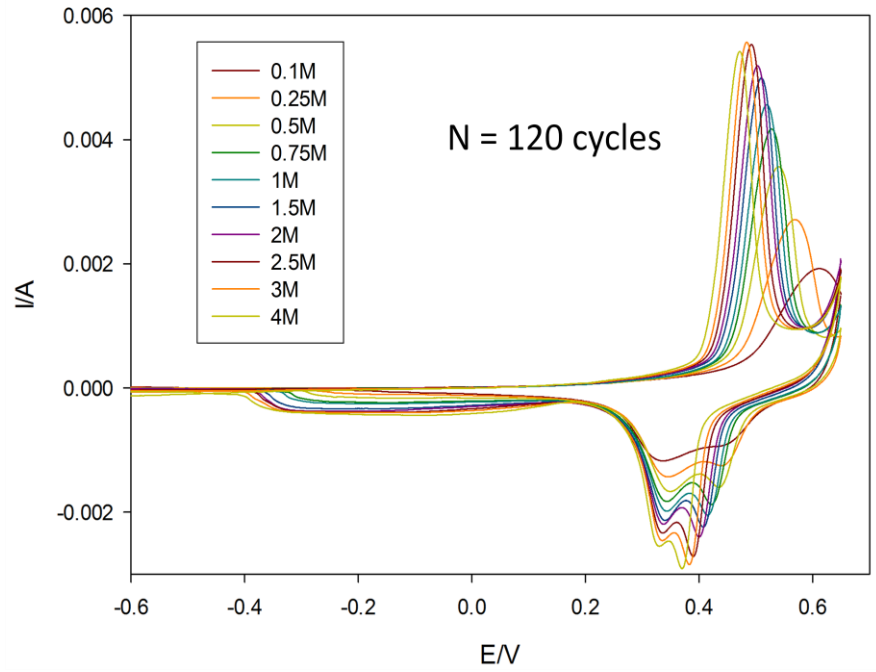

Figure 8. Voltammetric behaviour of a multicycled (in 1.0 M NaOH for N = 30 cycles) oxide coated Ni electrode as a function of base concentration.

We may note a number of features of interest. First the peak potentials vary with number of potential cycles or in effect with oxide charge capacity. For instance, at a given hydroxide ion concentration, the A_2 peak potential shifts to a more anodic value as the oxide film becomes thicker. Secondly, for all layer thicknesses examined the A_2 peak potential shifted to less anodic values and the C_2 potential to more cathodic values with increase in base concentration whereas the C_2* peak potential shifted only slightly with increasing value of the latter. These trends are illustrated quantitatively in fig.9 for an oxidized Ni electrode subjected to 30 cycles and in fig.10 to 120 potential cycles. We indicate the variation of voltammetric peak potential both with [OH^-] and with solution pH, the latter being calculated using the following expression: $pH = -\log\left\{K_W / \gamma_{\pm} m_{OH^-}\right\}$, where $\gamma_{\pm}$ denotes the mean ionic activity coefficient for NaOH solutions taken from Robinson and Stokes [41], and m_{OH^-} is the molality of the hydroxide ion. We have taken K_W = 1.0 x 10^{-14}. Note also that no attempt was made here to account for changes in the activity of water. One major point may be discerned from the data presented in fig.9 and fig.10. The A_2/C_2 peaks corresponding to the α/γ Ni(II)/Ni(III) redox transition shift significantly with increase in OH^- activity or solution pH. In contrast the C_2* peak only shows a significant decrease in potential with increasing OH^- activity only in the range 0.1 to 1.0 M, and when the oxide layer is relatively thin (30 cycles). Thereafter the peak potential remains invariant with solution pH. For the more extensively multicycled film the C_2* peak potential remains invariant over the entire hydroxide ion activity range studies corresponding to a calculated pH range of 12.8 – 14.5. Burke and Twomey [42] have performed a similar set of experiments, but their focus was on more concentrated base concentrations from 1.0 to 6.0 M. They noted that the C_2 peak potential dropped in value to less anodic values than the C_2* potential (which again remained invariant with changes in hydroxide ion activity) at base concentration values greater than 3.5 M. We do not observe such an irregular variation however.

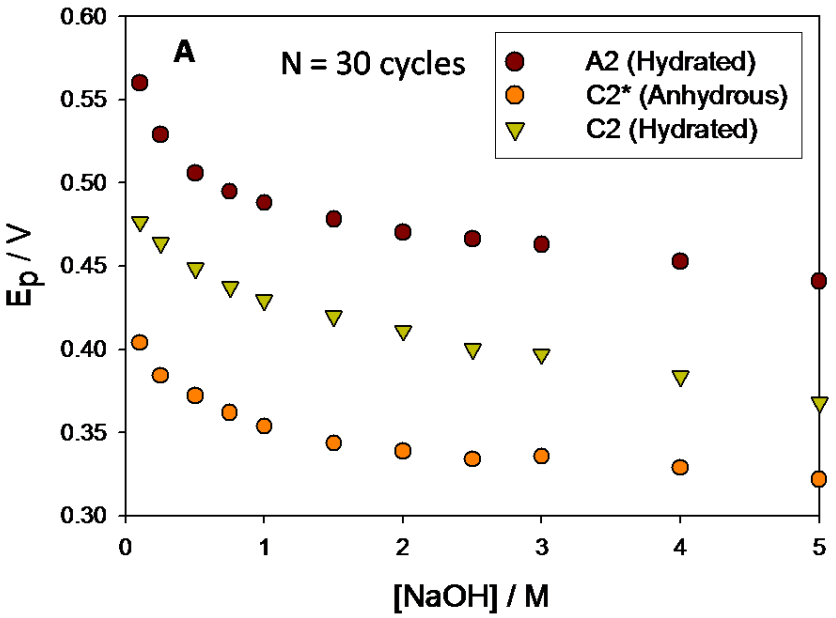

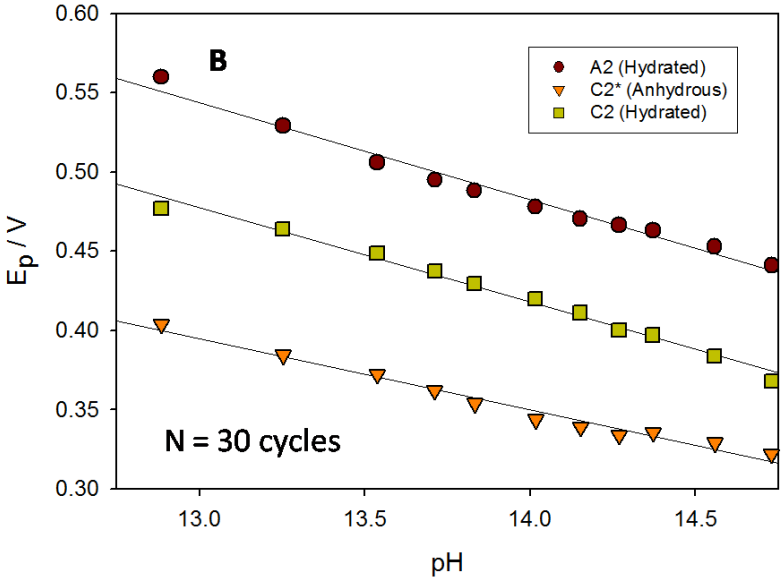

Figure 9. Voltammetric behaviour of a multicycled (in 1.0 M NaOH for N = 30 cycles) oxide coated Ni electrode as a function of base concentration. (A) Variation of peak potential with [OH^-]. (B) Variation of peak potential with calculated solution pH.

They note that a fresh electrode was used on changing from one solution to another. This procedure differs from the one employed in the present study in which the same oxide coated electrode was used in all base solutions examined. This factor may well account for the differences in detail noted. As will be noted subsequently when we discuss reaction order studies pertaining to the oxygen evolution reaction at oxidized Ni electrodes, less scattered kinetic data was obtained when the same oxide coated electrode in a single run in all base solutions . Hence we contend that it is a better experimental strategy to use the one film in a range of base solutions in a single run rather than using a freshly prepared oxide covered electrode for an individual solution of defined hydroxide ion activity.

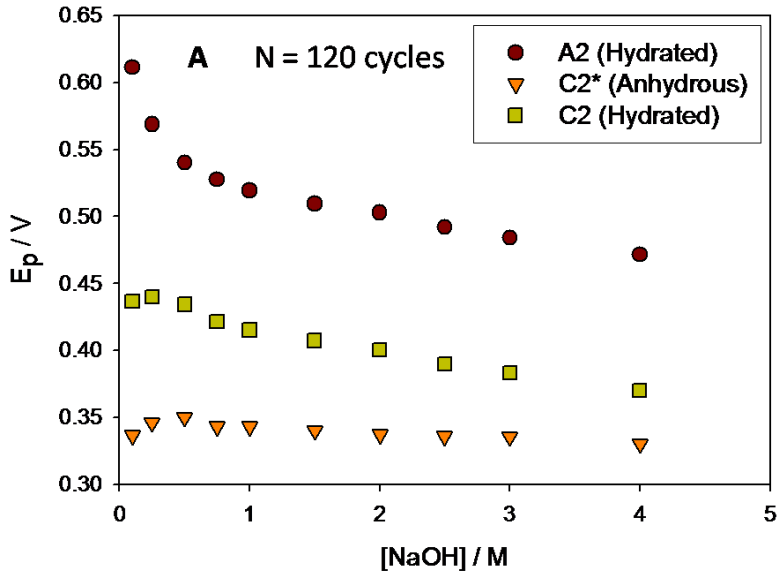

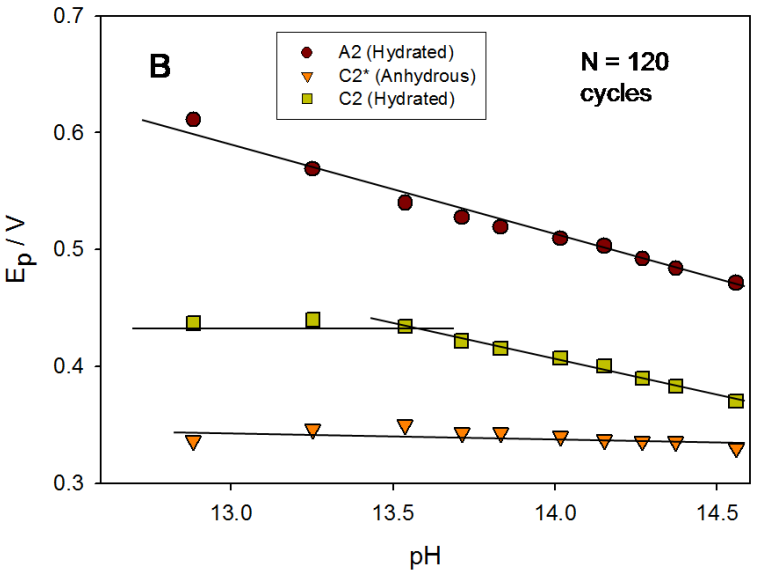

Figure 10. Voltammetric behaviour of a multicycled (in 1.0 M NaOH for N = 120 cycles) oxide coated Ni electrode as a function of base concentration. (A) Variation of peak potential with $[OH^-]$. (B) Variation of peak potential with calculated solution pH.

The values obtained for the variation of peak potential with decade change in calculated solution pH are interesting. For instance for peak A_2 : dE_p/dpH = - 0.061 V dec^{-1} for an oxide film grown for N = 30 cycles, whereas dE_p/dpH = - 0.079 V dec^{-1} for a thicker oxide film (N = 120 cycles). These numerical values are quoted with respect to the Hg/HgO reference electrode, which in our experiments is set up to be pH independent akin to the SHE. The behaviour observed for the C_2* peak is different. The peak potential decreases with increase in solution pH as $dE_P/dpH = -0.045V$ for an electrode modified with a relatively thin oxide layer (30 cycles). In contrast, the C_2* peak potential does not vary with solution pH when the electrode has been modified with a thick oxide layer. The latter zero shift in peak potential is quoted with respect to the Hg/HgO reference electrode scale. The behaviour of the C_2 peak is complicated. For electrodes modified with a thin oxide film (N = 30 cycles) the potential of the C2 peak decreases by ca. 0.060 V per decade change in pH (measured wrt to the Hg/HgO scale). In contrast, for electrodes modified with a thick hydrous oxide layer (corresponding to N = 120 cycles), we note that the potential does not shift with pH when data is taken in dilute base solution, but shifts in a manner similar to that observed for the A_2 peak in more concentrated base solution, where we note $dE_P/dpH = -0.061V$. It must be admitted that the pH range is narrow, but the shifts in voltammetric peak potential are very obvious as noted from the voltammograms presented in fig.7 and fig.8.

3.2 Analysis of redox switching within the hydrous oxide layer

3.2.1. Potential Step Chronoamperometry

We now consider the results of a series of experiments, conducted to quantify the rate of

charge percolation through the hyrated layer. The redox switching reaction (associated with the A_2/C_2 voltammetric peaks) reflects the change in oxidation state of the film as a result of a potential perturbation. Redox centres immediately adjacent to the support electrode are directly affected by the electrode potential, whereas charge is further propagated along the oxy-iron polymer strands in the hydrous layer via a sequence of electron self exchange reactions between neighbouring oxy-metal sites. This process is envisaged to be analogous to redox conduction exhibited by electroactive polymer films. In the simplest terms this electron "hopping" may be modelled in terms of a diffusional process, and so the charge percolation rate may be quantified in terms of a *charge transport diffusion coefficient*, D_{CT}. In the case of hydrous iron oxide, the latter may reflect either the electron hopping rate or the diffusion of of OH^- (or equivalently H_3O^+) ions via a rapid Grotthus type mechanism. The charge transport diffusion coefficient may be quantitatively estimated using cyclic voltammetry and potential step chronoamperometry.

As previously noted the charge/discharge reaction involving a Ni(II)/Ni(III) redox transition within the hydrous oxide is simplistically viewed as a $Ni(OH)_2/NiOOH$ transition of the type outlined in eqn.14. MacArthur [43], Zimmerman and Effa [44] Weidner and co-workers[45] and Mao et al [46] have suggested that the charge/discharge process is controlled by the diffusion of protons. We suggest that the latter occurs within the hydrated layer. Hence during discharge a proton diffuses from the film/electrolyte interface into the hydrous oxide region and an electron enters across the conducting compact oxide/hydrous film interface. During charging the proton diffuses to the film/electrolyte interface to react there with hydroxyl ions to form water. This idea is presented schematically in figure 11 below.

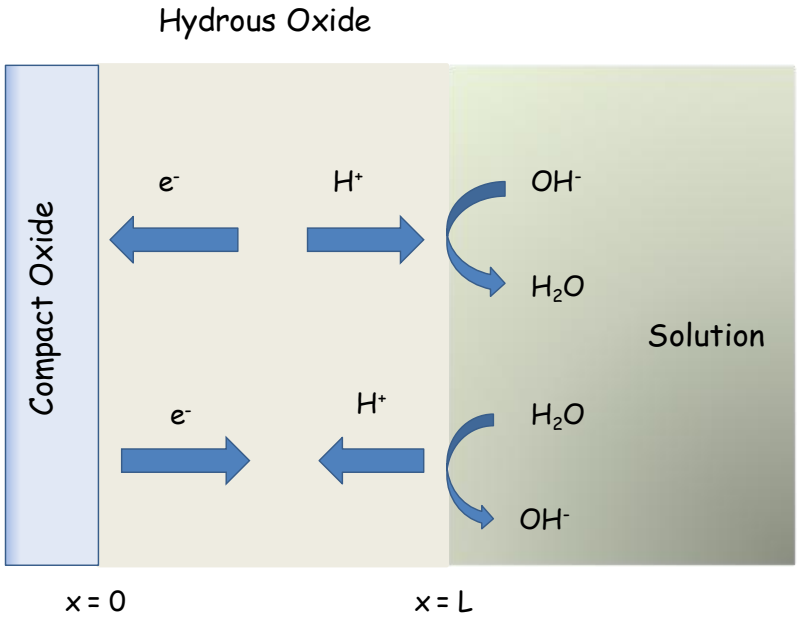

Figure 11. Schematic representation of charge/discharge redox switching mechanism occuring within the microdispersed hydrous nickel oxide layer. The thickness of the hydrous layer is L. The redox switching mechanism involves proton diffusion within the film coupled with chemical reaction at the outer interface.

We initially examine the response of the $Ni(OH)_2$/NiOOH system to a step in potential and compute theoretical expressions both for the chronoamperometric and chronocoulometric responses as a function of time. We focus attention of the diffusion of protons through the hydrous layer and their reaction at the outer film/solution interface. This process is of course accompanied by the Ni(II)/Ni(III) redox transformation which is described , to a first approximation as an electron hopping process between adjacent Ni sites in the hydrous film. Hence we apply a potential step of amplitude ΔE and monitor either the current response or the charge response as a function of time. The diffusion of protons in the hydrous layer is described by the Fick diffusion equation given by:

$$\frac{\partial c}{\partial t} = D\frac{\partial^2 c}{\partial x^2} \tag{15}$$

The following initial and boundary conditions apply

$$\begin{aligned} &t = 0 \quad c = c_\Sigma \\ &x = 0 \quad \left(\frac{dc}{dx}\right)_{x=0} = 0 \\ &x = L \quad f_\Sigma = -D\left(\frac{dc}{dx}\right)_{x=L} = kc = \frac{i}{nFA} \end{aligned} \tag{16}$$

Note this boundary value problem is different to that defining the electron hopping mechanism involving the Ni sites in the layer. In the latter problem kinetics at the x = L boundary are not considered and we have:

$$\begin{aligned} &t = 0 \quad c(x,0) = c_\Sigma \\ &x = 0 \quad c(0,t) = 0 \quad f_\Sigma = -D\left(\frac{dc}{dx}\right)_{x=0} = \frac{i}{nFA} \\ &x = L \quad \left(\frac{dc}{dx}\right)_{x=L} = 0 \end{aligned} \tag{17}$$

We now introduce the following normalized variables:

$$u = \frac{c}{c_\Sigma} \quad \chi = \frac{x}{L} \quad \tau = \frac{Dt}{L^2} \quad \lambda = \frac{kL}{D} \tag{18}$$

In the latter expression u denotes a normalised concentration of protons within the hydrous layer, χ defines the normalised distance, τ is the normalised time and λ defines the balance between reaction kinetics at the outer interface (or indeed within the aqueous pores in the layer) and the

diffusive rate in the layer. Note also that D is the diffusion coefficient of protons in film, k defines a pseudo first order rate constant and c_Σ is the total proton concentration in the layer. Translating the boundary value problem defined by eqn.15 and eqn.16 into normalized variables produces:

$$\begin{aligned}
&\frac{\partial u}{\partial \tau} = \frac{\partial^2 u}{\partial \chi^2} \\
&\tau = 0 \quad u(\chi, 0) = 1 \\
&\chi = 0 \quad \left(\frac{du}{d\chi}\right)_{\chi=0} = u_0' = 0 \\
&\chi = 1 \quad \Psi = \frac{Li}{nFADc_\Sigma} = \left(\frac{du}{d\chi}\right)_{\chi=1} = -\lambda u_1
\end{aligned} \tag{19}$$

The problem is most readily solved using the method of Laplace Transformation. Hence the Fick diffusion equation takes the following form in Laplace space:

$$p\bar{u} - 1 = \frac{d^2\bar{u}}{d\chi^2} \tag{20}$$

Where we have noted that $u(\chi, 0) = 1$. We may readily show that:

$$\begin{aligned}
&\bar{u} = \frac{1}{p} + A\cosh\left[\sqrt{p}\chi\right] + B\sinh\left[\sqrt{p}\chi\right] \\
&\frac{d\bar{u}}{d\chi} = \sqrt{p}A\sinh\left[\sqrt{p}\chi\right] + \sqrt{p}B\cosh\left[\sqrt{p}\chi\right]
\end{aligned} \tag{21}$$

Now when $\chi = 0$ $\bar{u}_0' = 0$ and so $B = 0$. Furthermore when $\chi = 1$ $\bar{u}_1' = -\lambda\bar{u}_1$. Also $\bar{u}_1' = \sqrt{p}A\sinh\left[\sqrt{p}\right]$. Furthermore we note that: $\bar{u}_1 = p^{-1} + A\cosh\left[\sqrt{p}\right] = -\lambda\bar{u}_1'$, and simplifying the latter expression and solving for A we get: $A = \left\{p\left(\cosh\left[\sqrt{p}\right] + \lambda^{-1}\sqrt{p}\sinh\left[\sqrt{p}\right]\right)\right\}^{-1}$. Hence the expression for the reaction flux in Laplace space is given by:

$$\left(\frac{d\bar{u}}{d\chi}\right)_{\chi=1} = \bar{\Psi} = \sqrt{p}A\sinh\left[\sqrt{p}\right] = \frac{\sqrt{p}\sinh\left[\sqrt{p}\right]}{p\left(\cosh\left[\sqrt{p}\right] + \lambda^{-1}\sqrt{p}\sinh\left[\sqrt{p}\right]\right)} \tag{22}$$

This expression may be further simplified to yield:

$$\bar{\Psi} = \left(\frac{d\bar{u}}{d\chi}\right)_{\chi=1} = \frac{\tanh\left[\sqrt{p}\right]}{\sqrt{p}\left(1+\lambda^{-1}\sqrt{p}\tanh\left[\sqrt{p}\right]\right)} \qquad (23)$$

We can examine various limiting forms of the general result expressed in eqn.23. We first examine the situation where the reaction/diffusion parameter λ is large which corresponds to the case of fast kinetics and one may consider ion transport in the hydrous layer to be slow and rate determining. This is a very common situation and especially so for proton transport hydrous oxide layers where the reaction between H^+ and H_2O is expected to be finetically facile. Under these circumstances $\lambda^{-1} \to 0$ and eqn.23 reduces to:

$$\bar{\Psi} = \left(\frac{d\bar{u}}{d\chi}\right)_{\chi=1} \cong p^{-1/2}\tanh\sqrt{p} \qquad (24)$$

Taking the inverse Laplace Transform of eqn.24 produces the following expressions for the chronoamperometric response:

$$\begin{aligned}\Psi(\tau) = \left(\frac{du}{d\chi}\right)_{\chi=1} &= \frac{1}{\sqrt{\pi\tau}}\sum_{m=0}^{\infty}(-1)^m\left\{\exp\left[-\frac{m^2}{\tau}\right]-\exp\left[-\frac{(1+m)^2}{\tau}\right]\right\} \\ &= \frac{1}{\sqrt{\pi\tau}}\left\{1+2\sum_{m=1}^{\infty}(-1)^m\exp\left[-\frac{m^2}{\tau}\right]\right\}\end{aligned} \qquad (25)$$

These expressions define the so called finite Cottrell equation for diffusion is a finite region.

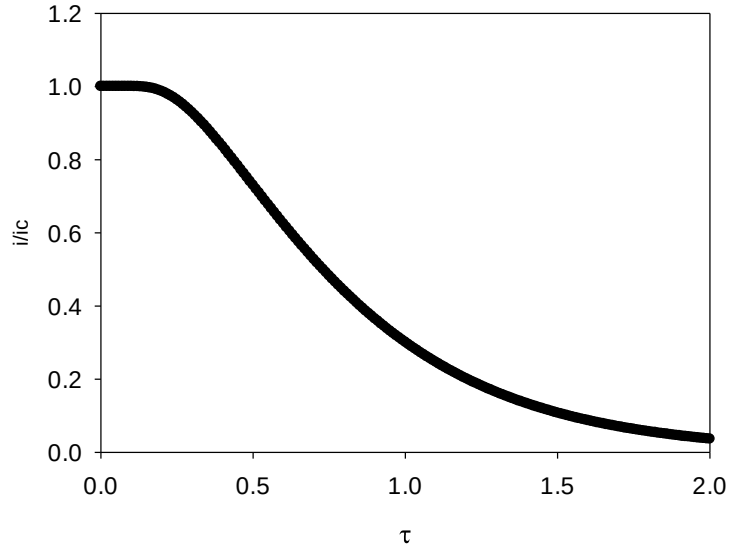

Figure 12. Variation of normalised current response (defined in terms of the ratio of the current response at any time to that corresponding to the Cottrell equation at that same time) with normalised time $\tau = Dt/L^2$.

We can show that eqn.25 may be written as:

$$i(t)=\left(\frac{D}{\pi t}\right)^{1/2}\frac{\Delta Q}{L}\left\{1+2\sum_{m=1}^{\infty}(-1)^m\exp\left[-\frac{m^2L^2}{Dt}\right]\right\} \tag{26}$$

In the latter expression the charge passed during the transient is $\Delta Q = nFAL\Delta c = nFA\Delta\Gamma$. The corresponding expression for the current when diffusion is semi-infinite is given by the Cottrell equation:

$$i_C(t)=\frac{1}{\sqrt{\pi t}}\left(\frac{D}{L^2}\right)^{1/2}\Delta Q \tag{27}$$

Hence from eqn.26 and eqn.27 we get:

$$\frac{i}{i_c}=\vartheta(\tau)=1+2\sum_{m=1}^{\infty}(-1)^m\exp\left[-\frac{m^2L^2}{Dt}\right]=\Theta_2\left(0\middle|Dt/L^2\right) \tag{28}$$

The latter expression has the form of a Theta function [47]. We illustrate eqn.28 in figure 12. Note that for short times $\vartheta\cong 1$ and the diffusion in the layer is semi-infinite in nature. Here at short times when $t<<D/L^2$ $\tau<<1$, the concentration polarization within the film does not reach the outside of the film and the simple Cottrell equation is valid.

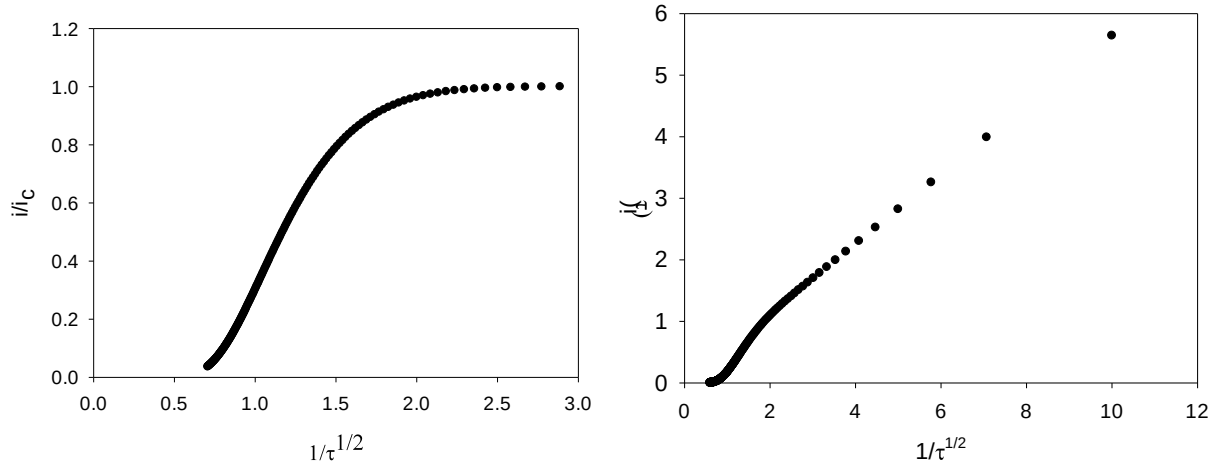

Figure 13. (a) Variation of normalised current response (defined in terms of the ratio of the current response at any time to that corresponding to the Cottrell equation at that same time) with the inverse square root of normalised time $\tau = Dt/L^2$. (b) Typical normalised Cottrell plot showing deviation from simple semi-infinite diffusion behaviour brought about by finite diffusion effects at longer times.

At longer times when $t \cong D/L^2$ $\tau \cong 1$ the concentration polarization in the hydrous layer reaches the outer surface and the diffusion limited current falls below that given by the Cottrell expression outlined in eqn.27. This may be noted from the working curves presented in figs. 12 and 13. The deviation from simple Cottrell behavior can be ascribed to the operation of the exponential terms in the infinite series presented in eqn.26.

We note that the chronoamperometric current transient is usually analysed by plotting i(t) vs $t^{-1/2}$ and fitting the experimental curve to the theoretical working curve illustrated above in fig.13(b). This fitting procedure can produce a value of the diffusive time constant D/L^2. Note that a value for the diffusion coefficient D can be estimated provided that the parameters ΔQ and L may be estimated.

Secondly, we examine the situation when transport within the hydrous layer is fast and the interfacial kinetics are slow. This corresponds to the case where the reaction/diffusion parameter λ is small. We return to eqn.23 and examine the limit of small p and large p corresponding to long and short experimental timescales respectively and derive approximate analytical expressions for the pertinent chronoamperometric current responses. Now when $p << 1$ we assume $\tanh\sqrt{p} \cong \sqrt{p}$ and the normalised current in Laplace Space is given by:

$$\bar{\Psi} = \bar{u}_1' \cong \frac{\sqrt{p}}{\sqrt{p}\left\{1+\frac{p}{\lambda}\right\}} = \frac{\lambda}{\lambda + p} \qquad (29)$$

Taking the inverse Laplace transformation we obtain:

$$\Psi = u_1' \cong \lambda \exp\left[-\lambda\tau\right] \qquad (30)$$

Hence a prediction of simple first order kinetics is proposed for the current decay during an applied potential step at long times, when transport within the hydrous film is rapid and interfacial kinetics at the film/solution interface is slow and rate determining. The situation pertaining in the short time regime is more complex. When $p >> 1$ we set $\tanh\left[\sqrt{p}\right] \cong 1$ in eqn.23 to obtain:

$$\bar{\Psi} = \bar{u}_1' \cong \frac{\lambda}{\sqrt{p}\left\{\lambda + \sqrt{p}\right\}} \qquad (31)$$

Again taking the inverse Laplace Transform of eqn.31 we obtain:

$$\Psi = u_1' \cong \lambda \exp\left[\lambda^2\tau\right] erfc\left[\lambda\sqrt{\tau}\right] = \lambda F\left(\lambda,\tau\right) \qquad (32)$$

We note that $F\left(\lambda,\tau\right) \to 0$ as $\tau \to \infty$. In contrast when $\tau = 0$, $F\left(\lambda,0\right) = 1$. The properties of

the function $F(\lambda,\tau)=\exp\left[\lambda^2\tau\right]erfc\left[\lambda\sqrt{\tau}\right]$ have been discussed by Spanier and Oldham [48]. We note that the function $\exp\left[\lambda^2\tau\right]$ increases rapidly in magnitude as the product $\lambda^2\tau$ increases, whereas the function $erfc\left[\lambda\sqrt{\tau}\right]$ suffers a dramatic decrease. The competition between these two opposing effects causes the product function $F(\lambda,\tau)$ to diminish in a very leisurely fashion towards zero as $\lambda\tau\to\infty$. Spanier and Oldham [48] note that an accurate approximation for the function $F(x)$ valid for all values of the product $x=\lambda^2\tau$ is :

$$F(x)=\exp[x]erfc\left[\sqrt{x}\right]\cong\frac{2}{\sqrt{\pi x}}\left\{\frac{1}{1+\sqrt{1+\frac{2}{x}\left(1-\frac{1-(2/\pi)}{\exp\left[\sqrt{5x/7}\right]}\right)}}\right\} \tag{33}$$

They note that the latter approximation exploits the following inequality valid for $\infty>x\geq 0$:

$$\frac{2}{1+\sqrt{1+\frac{2}{x}}}<\sqrt{\pi x}F(x)\leq\frac{2}{1+\sqrt{1+\frac{4}{\pi x}}} \tag{34}$$

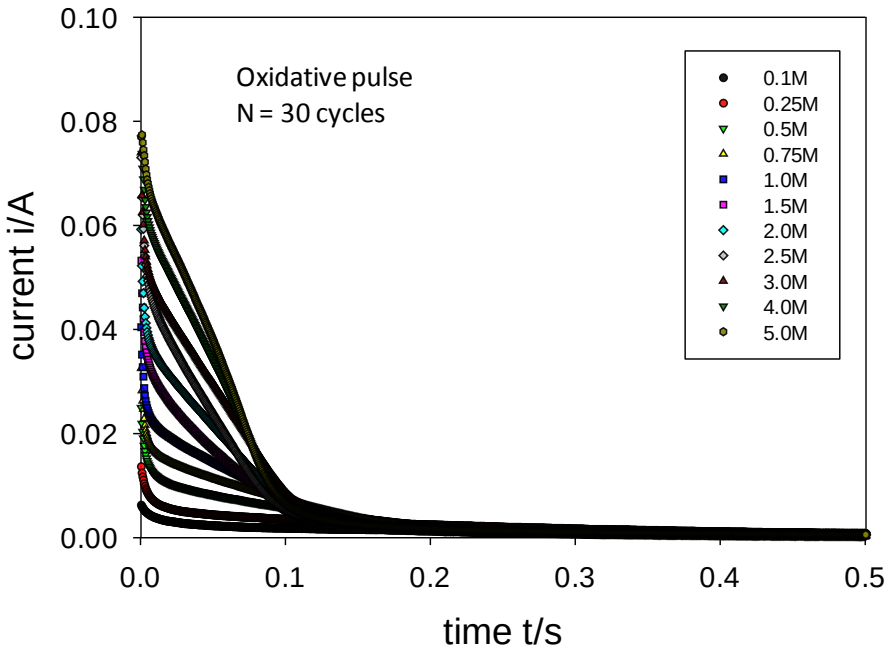

Figure 14. Typical current transients recorded as a function of hydroxide ion concentration for a multicycled Ni electrode (N = 30 cycles) after application of an oxidative potential step from 0.3 → 0.55 V (vs Hg/HgO).

Typical chronoamperometric response profiles to a double potential step perturbation to a multicycled Ni electrode (N = 30 cycles) in 1.0 M base are outlined in figure 14 and figure 15 below. below.

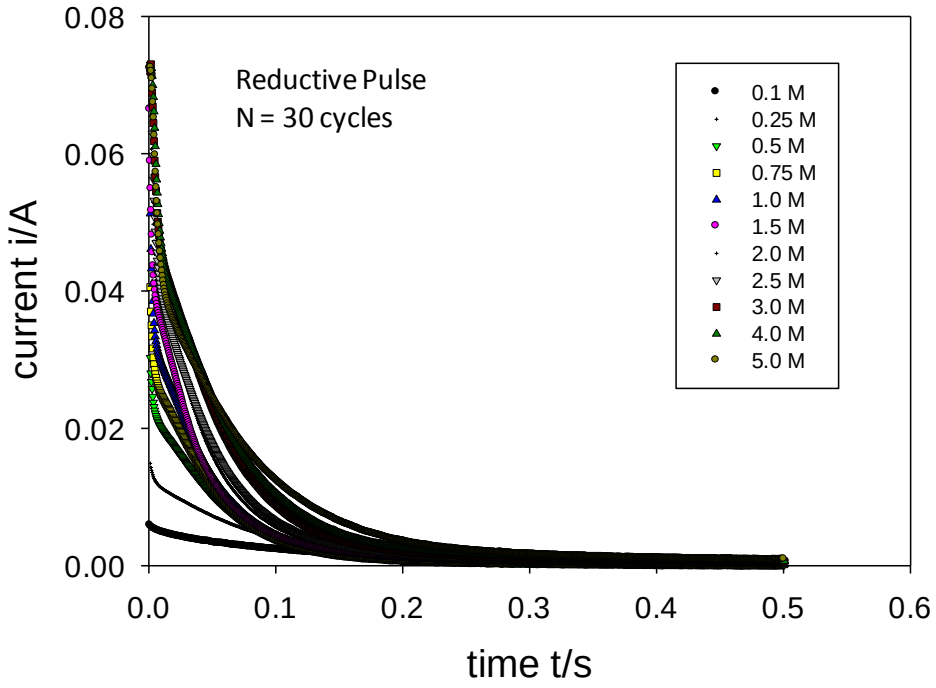

Figure 15. Typical current transients recorded as a function of hydroxide ion concentration for a multicycled Ni electrode (N = 30 cycles) after application of a reductive potential step from 0.55 → 0.30 V (vs Hg/HgO).

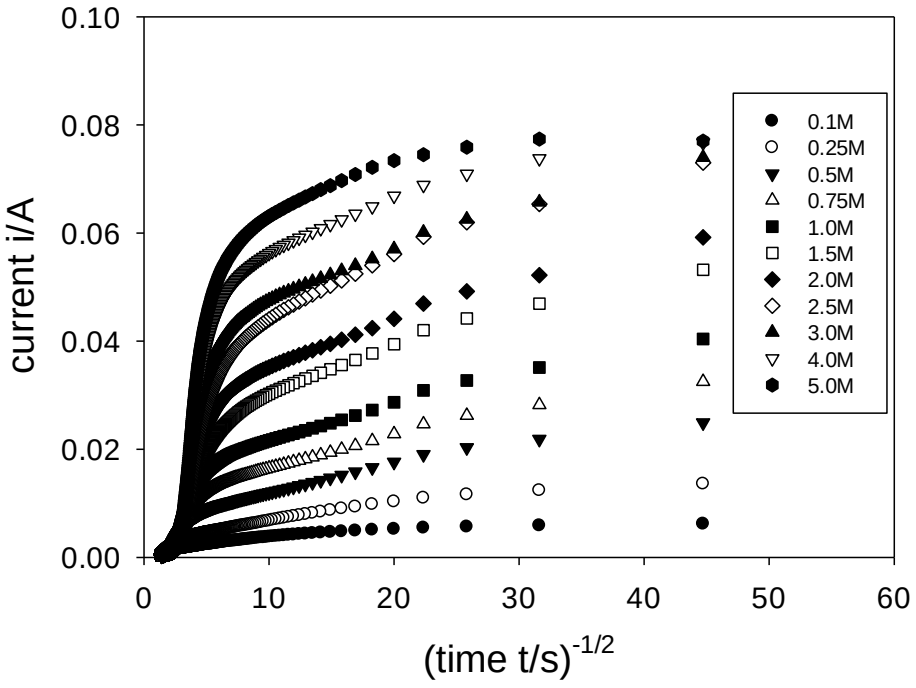

Figure 16. Cottrell analysis of oxidative PSCA data presented in fig.14.

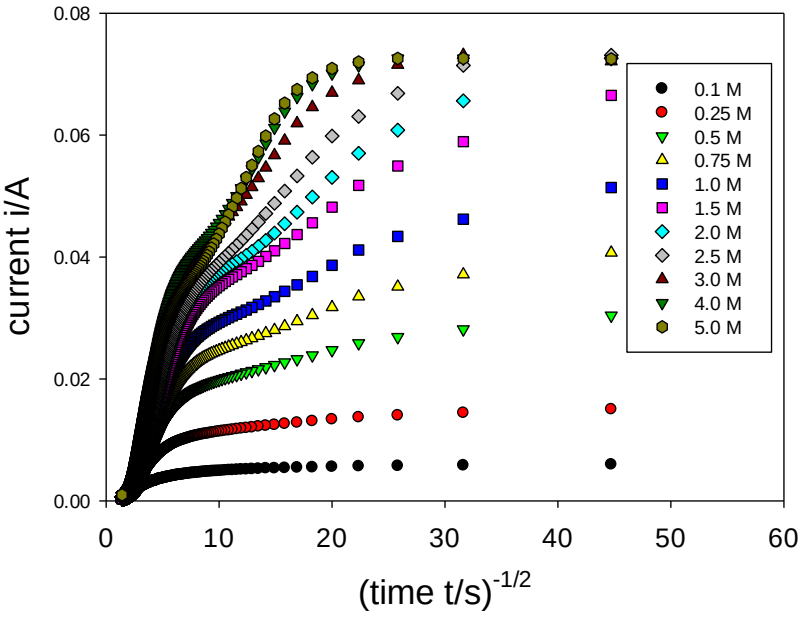

Figure 17. Cottrell analysis of reductive PSCA data presented in fig.15.

It is clear that the shape of the current transients are complex both for the oxidative and reductive potential steps. Simple current decay curves are only observed for potential steps performed only in the most dilute solutions. The response profiles deviate from simple decay when the experiment is performed in more concentrated base solution. The oxidative and reductive profile shapes also differ from one another.

The chronoamperometric transients presented in fig.14 and fig.15 are re-plotteed in Cottrell format in fig. 16 and fig. 17. The latter experiments clearly indicate that simple Cottrellian finite diffusion behaviour coupled with interfacial kinetics at the film/solution interface as discussed previously may not provide a complete representation of the situation, even if the hydrous oxide layer is relatively thin (layer generated after 30 potential cycles). This contention is supported by the results obtained for thicker oxide films as presented in fig. 18-21.

Typical chronoamperometric response profiles to a double potential step perturbation applied across the main charge storage peaks are presented in figure 18 -21 below. The results for an oxidative potential step (0.30 → 0.55 V, 0.5 s pulse width) are presented in linear (fig.18) and semi-logarithmic (fig. 19) formats and the corresponding responses for the reductive step (0.55 → 0.30 V, 0.5 s pulse width) are outlined in fig. 20 and fig. 21 in the same formats. This data was collected for a variety of hydrous oxide film thicknesses and over a range of base concentration between 0.1 M – 5.0 M. Data for N = 30, 90 and 180 oxide growth cycles are presented here.

The results from the latter experiments require a detailed and careful analysis which will be presented in a forthcoming paper. For the present we are content to make the following general comments.

First, the transients are not of a simple type. Indeed the overall shape varies with the

hydrous oxide layer thickness (for a fixed base concentration), and when recorded for a fixed number of oxide growth cycles, with the magnitude of the hydroxide ion concentration.

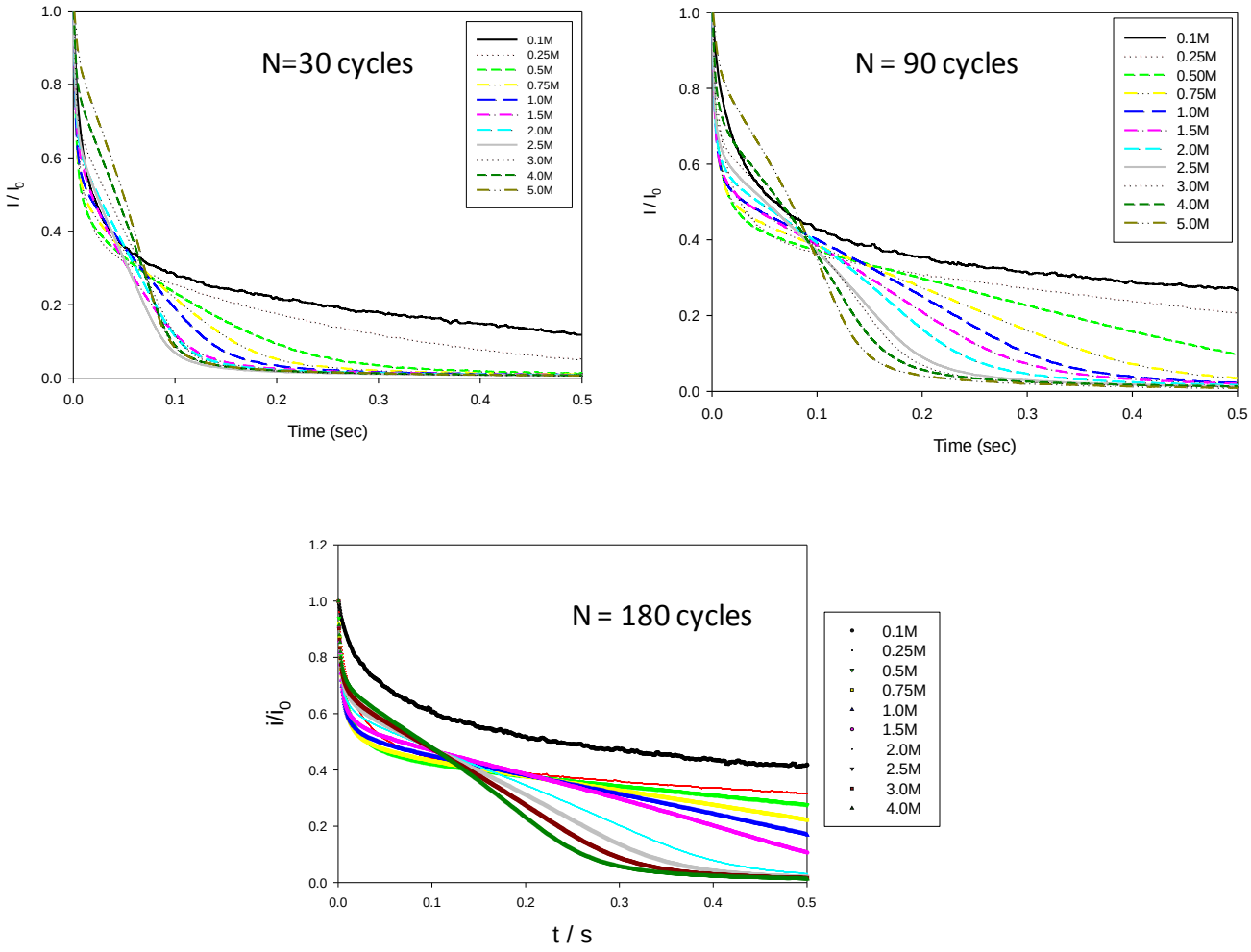

Figure 18. Normalised oxidative potential step chronoamperometry response transients (extracted from the first stage of a double potential step experiment of duration 0.5 s) recorded for hydrous oxide coated Ni electrodes which have been subjected to various numbers of oxide growth potential cycles in 1.0 M NaOH solution. In each case the transient is recorded in NaOH solutions of concentration in range 0.1 – 5.0 M.

Second, we note that a simple decay profile is observed only for transients recorded in the most dilute hydroxide ion solutions, typically between 0.1 – 0.5 M. For more concentrated base the decay curve is seen to conprise of two distinct regions: the first consisting of an initial decay followed by a a second, more pronounced region of more rapid current decay, the rate of which subsequently decreases at longer times.

Third, the reductive transients are less complex than those observed for the oxidative redox switching process. Indeed as oulined in fig. 16 the transients exhibit an initial rather rapid decay

which is essentially complete within the first 0.02 s of the pulse. This feature is then followed by a more gradual monotonically decreasing transient which persists over the remainder of the potential pulse. When the data is examined in semi-logarithmic format , three distinct linear regions may be discerned which are temporally well separated. The fine structure inherent in the transients becomes more obvious when the latter is recorded in more concentrated alkaline solutions.

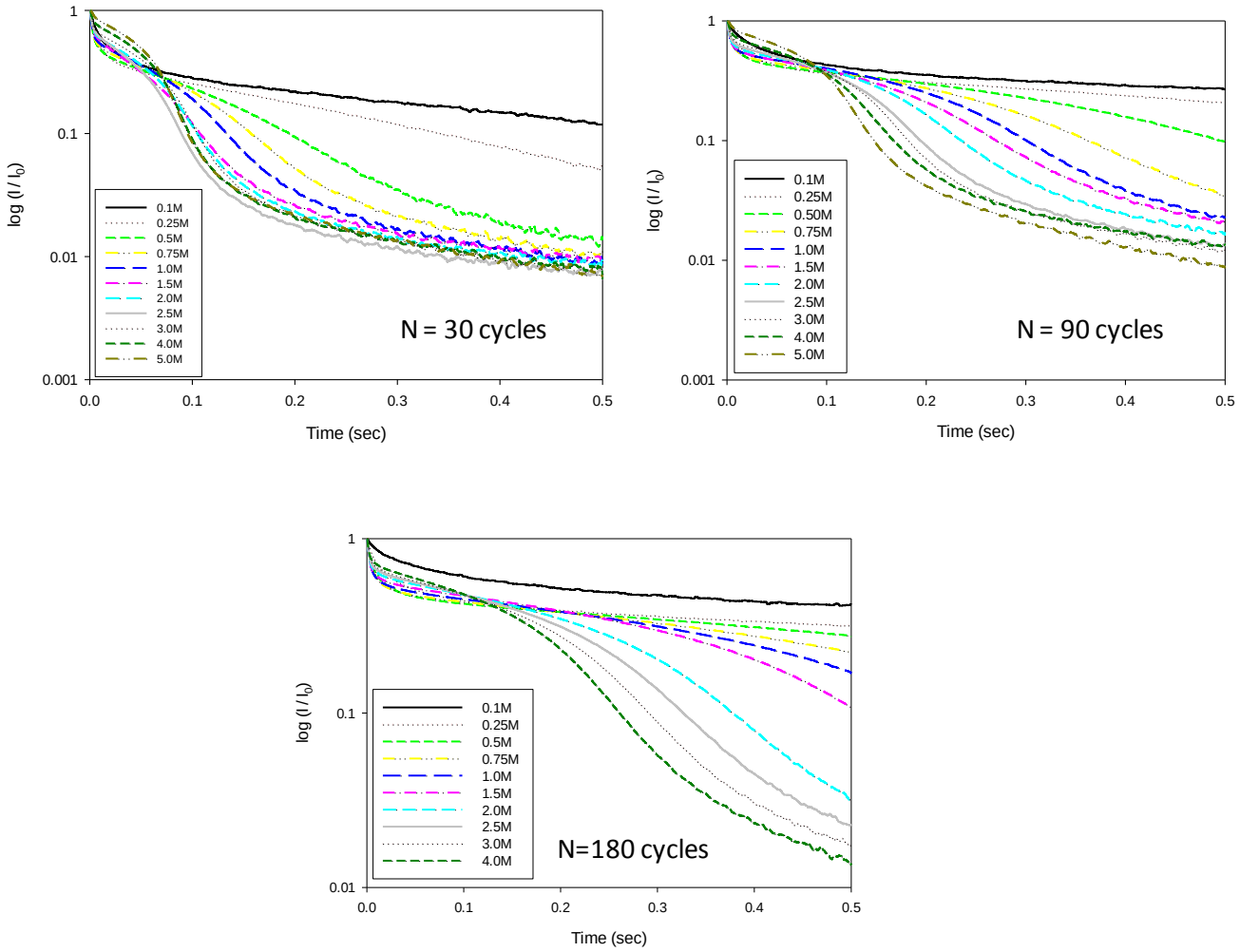

Figure 19. Normalised oxidative potential step chronoamperometry response transients (extracted from the first stage of a double potential step experiment of duration 0.5 s) recorded for hydrous oxide coated Ni electrodes which have been subjected to various numbers of oxide growth potential cycles in 1.0 M NaOH solution. The transient is recorded in semi-logarithmic format. In each case the transient is recorded in NaOH solutions of concentration in range 0.1 – 5.0 M.

Clearly the redox switching process is somewhat complex. This might perhaps not be totally unexpected since Weidner and co-workers [49] reported from galvanostatic charging and discharging experiments that the active material in nickel oxide electrodes cannot be fully accessed at high currents or for thick films. They proposed that the utilization of the active material is

controlled by the diffusion rate of protons through the film as outlined in fig. 11. The fraction of material utilized during charge (oxidative redox switching) is greater than that utilized during discharge (reduction). The latter asymmetry could be attributed to a proton diffusion coefficient that is a function of the state of charge of the active material. This clearly implies that the reaction/diffusion expression presented in eqn.19 must be modified along the lines suggested by Weidner and co-workers [49]. Furthermore, we recall fig.6 and note that structural transformations occur between the nickel oxides within the region of redox switching. It is therefore not unexpected that the chronoamperometric response will exhibit features that are reminescent of nucleation/growth transients seen during electrochemical phase formation processes. We will explore this issue in greater detail in a forthcoming paper.

One rather significant comment which we will make at this stage however is that although potential step chronoamperometry is perhaps the most simple of transient electrochemical techniques to employ practically, the current transient response profile is very sensitive to deviations from the simple predicted finite diffusive behaviour.

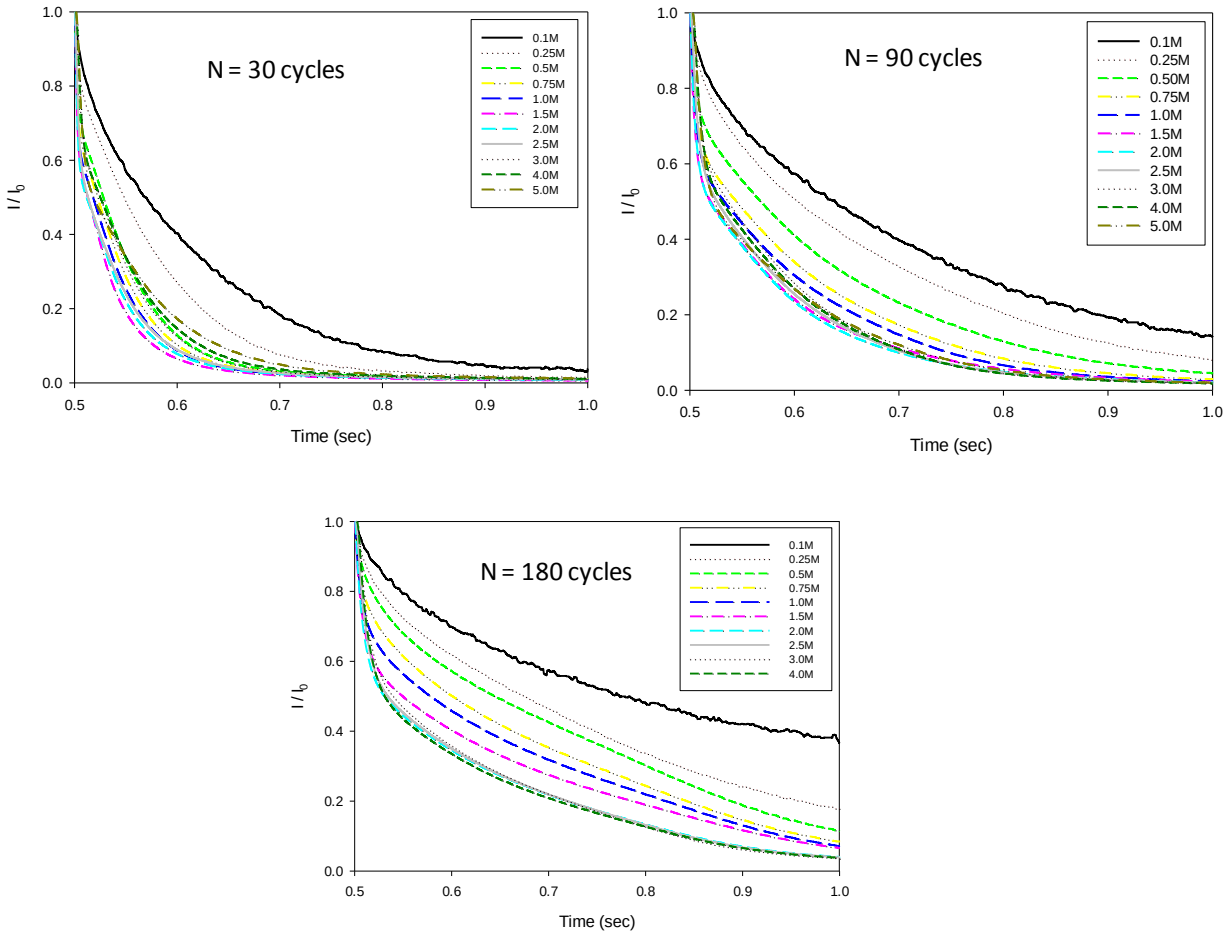

Figure 20. Normalised reductive potential step chronoamperometry response transients (extracted from the second stage of a double potential step experiment of duration 0.5 s) recorded for hydrous oxide coated Ni electrodes which have been subjected to various numbers of oxide growth potential cycles in 1.0 M NaOH solution. In each case the transient is recorded in NaOH solutions of concentration in range 0.1 – 5.0 M.

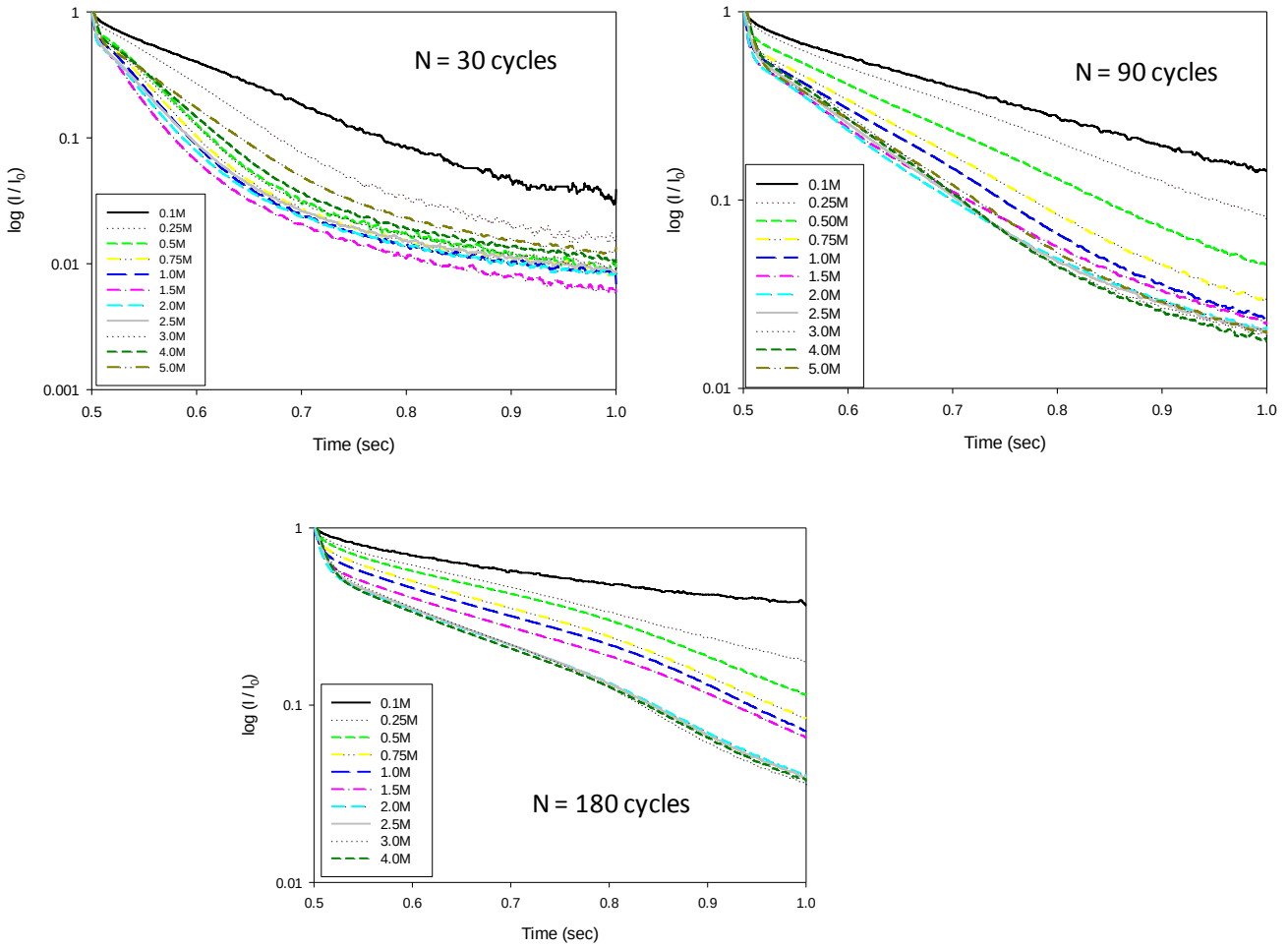

Figure 21. Normalised reductive potential step chronoamperometry response transients (extracted from the second stage of a double potential step experiment of duration 0.5 s) recorded for hydrous oxide coated Ni electrodes which have been subjected to various numbers of oxide growth potential cycles in 1.0 M NaOH solution. The transient is recorded in semi-logarithmic format. In each case the transient is recorded in NaOH solutions of concentration in range 0.1 – 5.0 M.

As such it is a very useful simple technique to employ in the study of oxide modified electrodes where redox switching can prove in some cases (such indeed as the present case) to be quite complex.

3.2.2 Potential Sweep Voltammetry

We now examine the redox switching behaviour of the hydrated nickel oxide electrode in aqueous base to a potential sweep perturbation. Although we have noted in the previous section that the redox switching proces may be somewhat more complex, we will attempt to apply a simple first order finite diffusion model to obtain quantitative transport information pertaining to the proton diffusion coefficient through the hydrous layer. In the present work we utilise the

mathematical formalism of Aoki and co-workers [50] and extended by others [51], to derive an expression for the inverse diffusive time constant $\tau_D^{-1} = D/L^2$. These workers solved the finite diffusion problem under conditions of a linear potential sweep. Transport information may be readily extracted from an analysis of the shape of the voltammetric response as a function of sweep rate. We have recently reported the utilization of this analysis to examine the redox switching process for multicycled iron electrodes in aqueous base [52].

We will apply the most simple variant of the Aoki model and consider the situation where the charge percolation along the oxide polymer strands between adjacent Ni sites and the accompanying proton diffusion in the pores can be considered to be irreversible. The conditions under which the latter conditions pertain may be discerned by examining the variation of the voltammetricp peak potential with sweep rate. The results of such an experiment is presented in fig. 22 below. Here the cyclic voltammetric response as a function of sweep rate is examined for various hydrated nickel oxide films of varying thickness (the latter scaling with the number of potential cycles employed during the layer growth process).

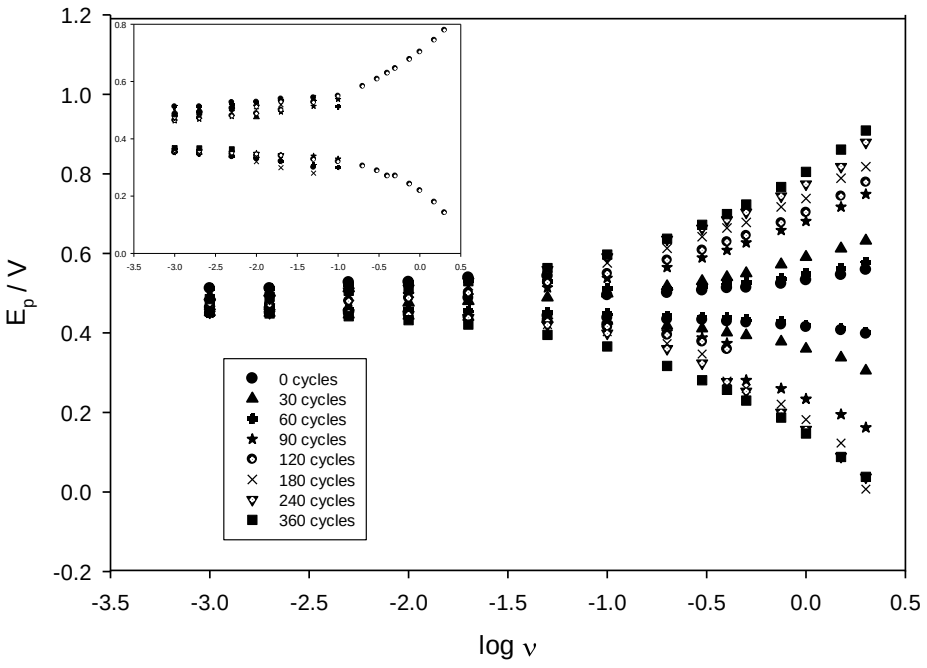

Figure 22. Variation of voltammetric peak potential with log sweep rate for a series of multicycled Ni electrodes in 1.0 M NaOH at 298 K. Attention is focused on the main anodic and cathodic charge storage peaks corresponding to the Ni(II)/Ni(III) redox transition located at potentials prior to active oxygen evolution.

In short, when the diffusive charge percolation process is reversible the voltammetric peak potentials will remain invariant with changes in sweep rate. In this way we define the time window in which the electrochemical reversibility pertains. We note that the peak potential begins to shift significajntly with increasing sweep rate for values greater than 1 Vs^{-1}. Between 0.3 Vs^{-1} and

1.0Vs^{-1} an intermediate transition region is observed. Below 0.3 Vs^{-1} the peak potential remains invariant with sweep rate and the redox switching reaction is regarded to be kinetically reversible.

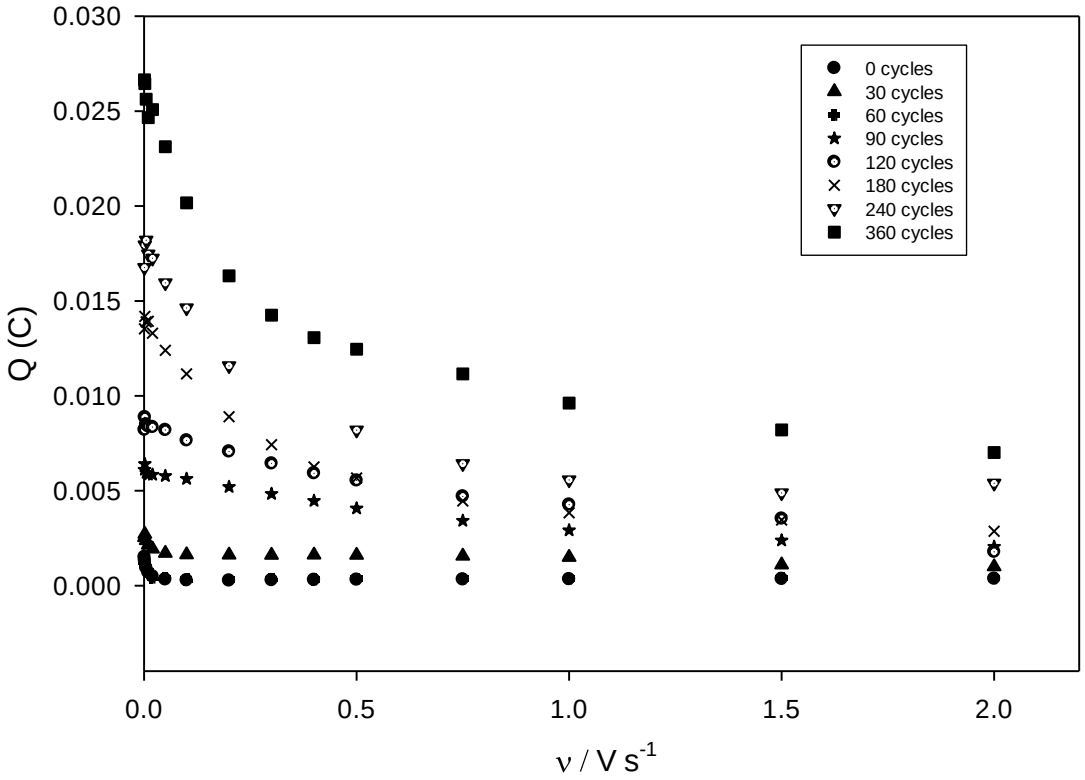

Figure 23. Variation of voltammetric redox charge capacity Q with analytical sweep rate for a series of Ni oxide hydrous films grown under potential cycling conditions for various number of cycles. Attention is focused on the main anodic charge storage peak corresponding to the Ni(II)/Ni(III) redox transition located at potentials prior to active oxygen evolution.

The variation of hydrous oxide charge capacity Q (which is proportional to the redox charge capacity C defined for electroactive polymer films in the work of Murray et al [53,54], with analytical sweep rate is presented in fig. 23. We note that the recorded charge capacity values for reasonably thin oxide films (less than 60 cycles growth) remain invariant with sweep rate between 2 Vs^{-1} until ca 10 mVs^{-1}, and then increase slightly as the sweep rate is decreased further. This trend is most marked for thicker films (180 cycles growth and greater). Indeed for a thick nickel oxide layer it may be noted that the charge capacity increases by nearly 50% when the sweep rate in decreases from ca. 1 Vs^{-1} to ca. 10 mVs^{-1}. A similar result has been recently noted for hydrous iron oxide films in base [52].

These results may be readily rationalised in terms of a simple diffusive model as previously noted [52]. With thinner films there is sufficient time at normal sweep rates for the redox reaction to extend to virtually all regions of the dispersed hydrous layer, i.e. a situation of Nernstian equilibrium pertains through the hydrous film, and the redox charge capacity will be effectively

independent of experimental time scale (i.e. sweep rate). However with thicker films there is not enough time (apart from the lowest sweep rates or alternatively longest time scales) for the redox reaction to propagate throughout the entire extent of the dispersed hydrous region. Thus the charge capacity values drop dramatically as the analytical sweep rate is increased.

The variation of voltammetric peak width at half peak height for the main anodic charge stroage peak A_2 with sweep rate is outlined in fig.24 below. We present data for a range of oxide film thicknesses. We note that in all cases examined the peak width at half peak height increases regularly with increasing sweep rate from an initial value of ca. 30 mV at the lowest values of sweep rate to considerably larger values at higher sweep rates. Furthermore it was noted that at a particular sweep rate the peak width at half peak height increased regularly with number of potential cycles.

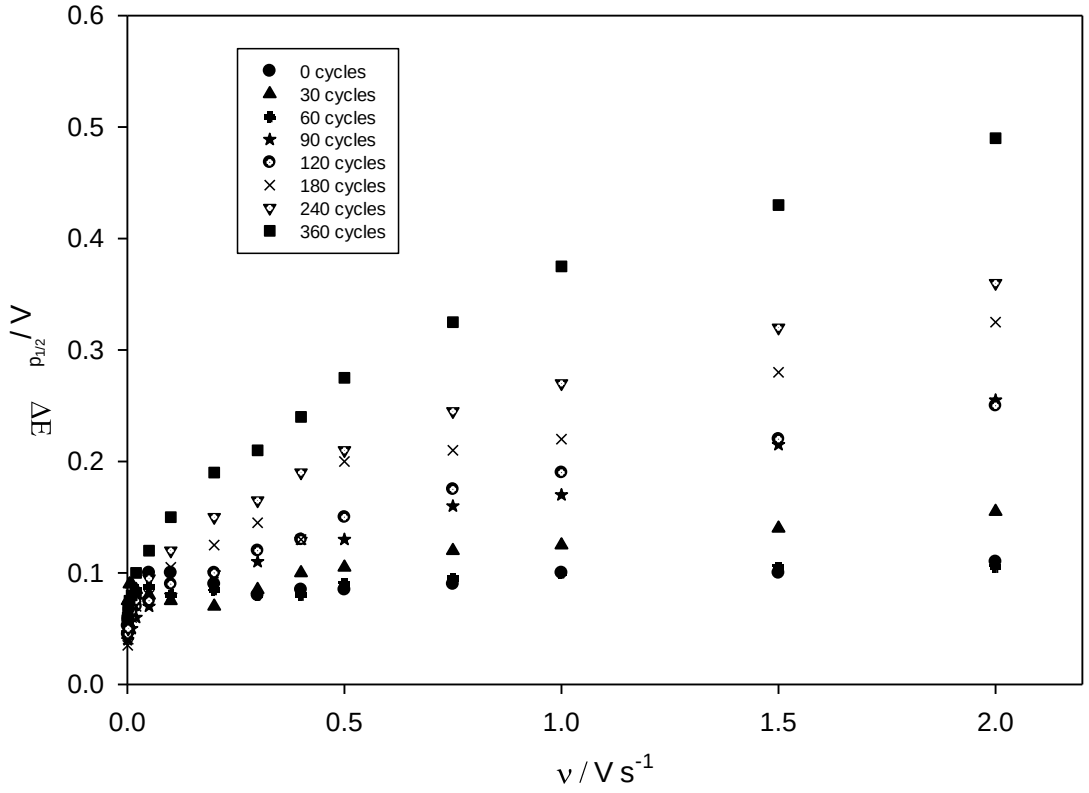

Figure 24. Variation of peak width at half peak height with sweep rate for a series of multicycled nickel electrodes in 1.0 M NaOH.

Lyons [55] has noted that the peak width at half peak height $\Delta E_{p/2}$ value extracted from the voltammogram recorded for an electrode chemically modified with an electroactive polymer thin film conveys very useful information about the electrochemistry of redox switching in the layer. Similar considerations arise in the present case. Laviron [56] has developed a useful theory to describe redox switching within space distributed electroactive redox polymer films where charge is transferred via nearest neighbour electron hopping both intrastrand and interstrand. The analysis

has been further extended by Aoki and co-workers [50]. These models enable the cyclic voltammetric response to be analysed quantitatively as a function of sweep rate. In particular these models enable a prediction to be made concerning the shape of the voltammetric response both for reversible, totally irreversible and indeed quasi-reversible redox switching reactions occuring both in monolayer and multilayer modified electrodes thin films, both in the absence of and in the presence of interactions between the participating redox centers. These models have been well described by Lyons [55]. In the latter models, if it is assumed that redox switching is electrochemically reversible then the peak width at half peak height is assumed to be given by:

$$\Delta E_{p/2} = \frac{2RT}{nF}\ln\left(3+2\sqrt{2}\right) = \frac{3.53RT}{nF} \qquad (35)$$

Keeping in mind the representation of the Ni(II)/Ni(III) redox switching reaction presented in scheme A previously we can assign n= 2 and for T=298 K we predict that $\Delta E_{p/2} \cong 45.3mV$ which is in excellent agreement with the experimental data recorded in fig.24 in the low sweep rate limit. Now in many situations it is established that voltammetric peaks are either broader or narrower than this ideal value. This observation implies that either repulsive or attractive interactions operate within the thin film. Furthermore such as occurrence signifies that either not all sites in the film have the same standard potential or thermodynamic activity effects must be considered. Occupied redox sites with repulsive interactions tend to avoid one another, which ultimately promotes an alternating site occupancy; this is essentially the same as compound formation. This effect results in a broadening of the voltammetric peak response compared with that expected ideally as outlined in eqn.35 for a reversible reaction. In contrast when the interactions are attractive, occupied sites tend to cluster together, which leads to phase separation and considerable narrowing in the voltammogram compared with the ideal. In electroactive polymer materials the extent of peak broadening or narrowing depends to a great extent on the nature of the solvent and the identity and concentration of the charge compensating counterions.

According to Aoki [50] the peak width is related to an empirical interaction parameter σ as follows:

$$\Delta E_{p/2} = \frac{2RT}{nF}\left\{\ln\left(\frac{1+\rho}{1-\rho}\right) - \rho\sigma\right\} \qquad (36)$$

In the latter expression we note that $\sigma = gc_{\Sigma} = g\Gamma/L = G/RT$ where g denotes the Temkin interaction parameter which is negative if repulsive interactions operate and positive if attractive interactions pertain, and G denotes the Gibbs energy of interaction between the redox sites[2]. Furthermore, $c_{\Sigma} = \Gamma/L$ denotes the site concentration within the hydrous layer, and Γ, L represents

[2] If g = 0 the peak has the shape and characteristics of the ideal Langmuirian voltammetric peak. If g < 0, the peak becomes broader and flatter, and if g > 0, with 0 < g < 2, the peak becomes narrower and sharper. If g > 2 a hysteresis phenomenon is exhibited and the peaks can no longer be described mathematically.

the surface coverage and layer thickness respectively. Furthermore we note that:

$$\rho = \sqrt{\frac{2-\sigma}{4-\sigma}} \tag{37}$$

Under reversible conditions the voltammetric peak corresponding to the redox switching reaction within the hydrous oxide layer is identical in shape to the theoretical reversible monolayer peak for reasonably slow sweep rates[3]. The fact that the peak width at half peak height indicates that the voltammetric peaks exhibit an increasingly more prominent 'tailing' effects as the experimental timescale decreases, in which the peaks exhibit an increasing asymmetry about $E\text{-}E_p$. The latter occurrence may be attributed to the fact that there is not enough time at faster sweep rates at the beginning of the scan for the redox reaction to propagate through the film. This of course is a diffusive effect.

Aoki has shown that the voltammetric response for a thin film in which the redox reaction is reversible takes the following form:

$$i = nFA(\Gamma/L)\sqrt{nFD\upsilon/RT}\, W^{1/2}\int_0^{\infty}\theta_2(0,y)\frac{\exp\left[Wy-\xi(\tau)\right]}{\left(1+\exp\left[Wy-\xi(\tau)\right]\right)^2}dy = nFA(\Gamma/L)\sqrt{nFD\upsilon/RT}\,F(W,\xi) \tag{38}$$

Where we have set:

$$F(W,\xi) = W^{1/2}\int_0^{\infty}\theta_2(0,y)\frac{\exp\left[Wy-\xi(\tau)\right]}{\left(1+\exp\left[Wy-\xi(\tau)\right]\right)^2}dy \tag{39}$$

In the latter expression we note that:

$$\xi(\tau) = \frac{nF}{RT}\left(E_i - E^0\right) + \frac{nFL^2\upsilon\tau}{RT} \tag{40}$$

Also we note that $\tau = Dt/L^2$, and we introduce the Theta function as:

$$\theta_2(0,y) = \frac{1}{\sqrt{\pi y}}\left\{1+2\sum_{k=1}^{\infty}(-1)^k\exp\left[-\frac{k^2}{y}\right]\right\} \tag{41}$$

We also note that the parameter W is given by:

---

[3] This is given by the expression $\Psi = \mathrm{sech}^2\left[\xi/2\right] = \exp\left[-\xi\right]/\left(1+\exp\left[-\xi\right]\right)^2$ where the normalized current response is given by $\Psi = i/\left(nF^2A\Gamma\upsilon/RT\right)$ and the normalized potential is $\xi = nF(E-E^0)/RT$.

$$W = \frac{nFL^2\upsilon}{DRT} = \left(\frac{L}{X_D}\right)^2 \tag{42}$$

And the diffusion layer thickness is:

$$X_D = \sqrt{\frac{DRT}{nF\upsilon}} \tag{43}$$

Hence we note that the parameter $\sqrt{W}$ is simply the ratio of the layer thickness to the diffusion layer thickness in the film. Now the general expression outlined in eqn.38 cannot be integrated analytically, so one must resort to a numerical analysis in order to compute the shape of the voltammogram. However eqn.38 must reduce to the surface voltammetic limit when W is small and to the semi-infinite Randles-Sevcik limit when the parameter W is large. Hence:

$$\lim_{W\to 0}\left\{W^{-1/2}F(W,\xi)\right\} \to \frac{\exp[-\xi]}{\left(1+\exp[-\xi]\right)^2}\int_0^\infty \theta_2(0,y)\,dy \to \frac{\exp[-\xi]}{\left(1+\exp[-\xi]\right)^2} \tag{44}$$

The result presented in eqn.44 is obtained since we note that:

$$\int_0^\infty \theta_2(0,y)\,dy = \lim_{p\to 0}\left\{L\left(\theta_2(0,\tau)\right)\right\} = \lim_{p\to 0}\left\{p^{-1/2}\tanh\left[\sqrt{p}\right]\right\} = 1 \tag{45}$$

Where p is the Laplace parameter. Furthermore if W is large enough such that semi-infinite diffusion conditions pertain, then in this case we can show that the Theta function in eqn.38 reduces to:

$$\theta_2(0,y) \cong \frac{1}{\sqrt{\pi y}} \tag{46}$$

And the expression for the current reduces to:

$$i \cong nFA(\Gamma/L)\sqrt{\frac{nFD\pi}{RT}\upsilon}\int_0^\infty \frac{\exp[Wy-\xi]}{\left(1+\exp[Wy-\xi]\right)^2}\,y^{-1/2}dy \tag{47}$$

This integral equation is essentially similar in form to that derived many years ago by Nicholson and Shain and others [57,58]. The latter integral may be evaluated numerically and we may readily show that the peak current is given by:

$$i_P = 0.4463nFA\Gamma\sqrt{\frac{nF}{RT}}\left(\frac{D}{L^2}\right)^{1/2}\upsilon^{1/2} \tag{48}$$

This is the well established Randles-Sevcik expression characteristic of semi-infinite diffusion. Hence the diffusive time constant $\tau_D = \frac{D}{L^2}$ can be evaluated from the slope of the Randles-Sevcik plot.

The variation of voltammetric peak current with square root sweep rate for a series of multicycled Ni electrodes in 1.0 M NaOH is outlined in fig.25 below. We note good Randles-Sevcik linearity at lower sweep rates but the current response begins to level out at higher sweep rates.

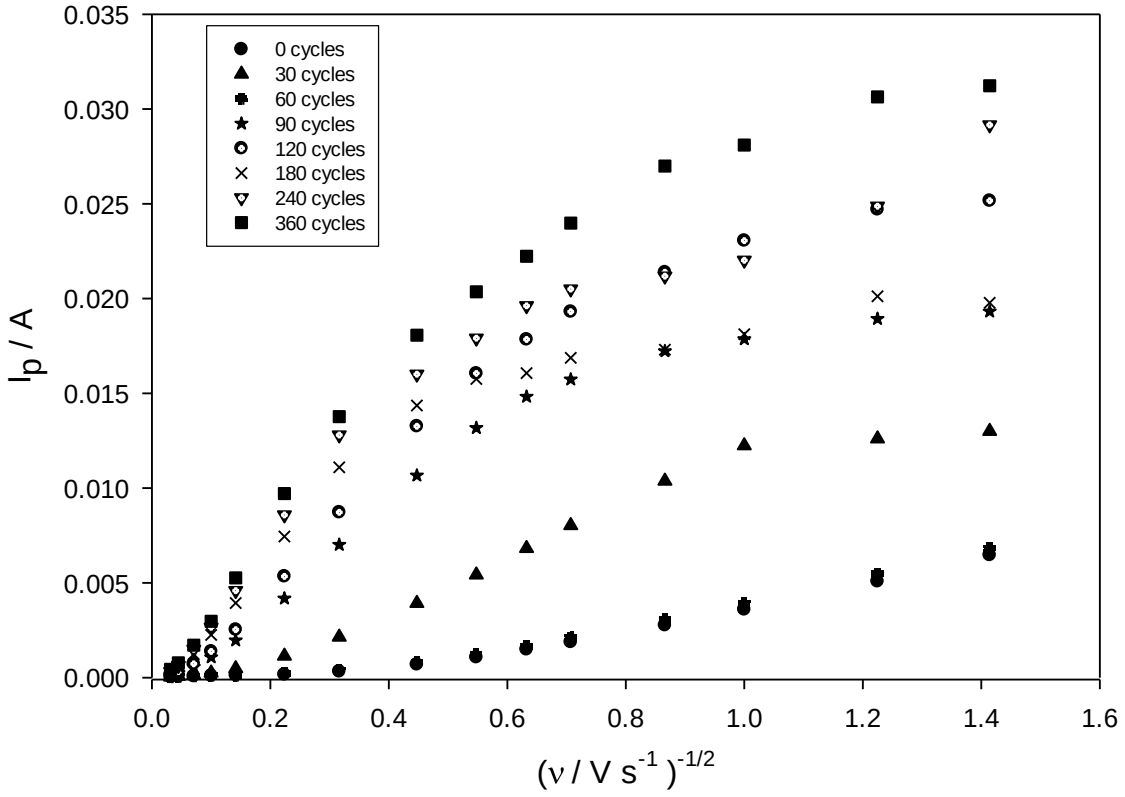

Figure 25. Typical Randles-Sevcik plots recorded for a series of multicycled Ni electrodes in 1.0 M NaOH as a function of number of oxide growth cycles.

This type of levelling out in the current response at high sweep rates can be predicted from the Aoki analysis [50]. In particular, using a numerical analysis it has been shown that the peak current, i_p, representing the main redox switching process in the hydrated layer varies with υ according to,

$$i_P = 0.446nFA\left\{\Gamma D/L^2\right\}W^{1/2}\tanh\left[\Upsilon\right] \qquad (49)$$

Where we note that:

$$\Upsilon = 0.56\sqrt{W} + 0.05W \qquad (50)$$

And we recall that W is defined via eqn.42. This expression may be re-cast in a non-dimensional format to produce a working curve as follows:

$$\Psi = \frac{i_P}{nFA(\Gamma/L)}\left\{\frac{RT}{nFD\upsilon}\right\}^{1/2} = 0.446\tanh[\Upsilon] \quad (51)$$

In fig.26 we plot eqn.51, and note that it shows a characteristic limiting plateau region similar to that reported in fig.25.

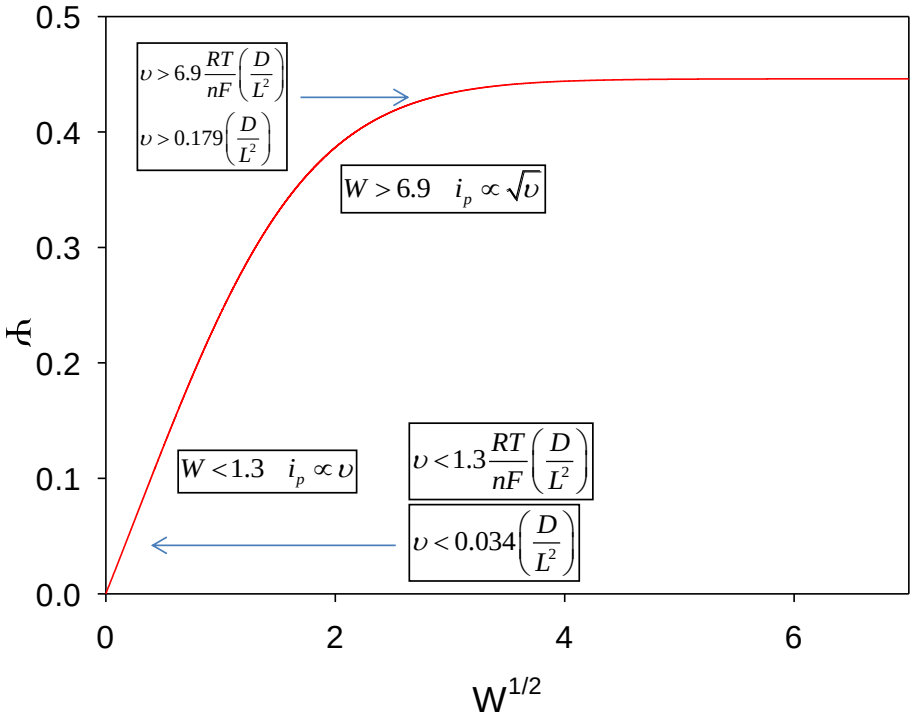

Figure 26. Variation of numerically evaluated dimensionless peak current Y with $\sqrt{W} = L/X_D$. Plot computed via eqn.51 using SigmaPlot software.

We note from the working curve presented in fig.26 that for W < 1.3 we obtain voltammetric profiles characteristic of surface type behaviour: the characteristic bell shape is observed; for W > 1 a marked diffusive tailing in the current response is observed, and the latter feature becomes more pronounced for large W values. We also note that peak current is proportional to squate root sweep rate for W > 7 and is directly proportional to sweep rate for W < 1.3. We also note for T = 298 K and n = 1 then $RT/nF \square 0.026V$. Hence under these conditions the lower limit of the sweep rate for observing semi-infinite diffusion effects is $0.18\tau_D$, and the upper limit for observing surface behaviour is $0.034\tau_D$.

The diffusive frequency $\tau_D = D/L^2$ can be readily evaluated via numerical analysis of eqn.49 via the following expression:

$$G(\tau_D) = \alpha \tau_D^{1/2} \tanh\left\{\beta \tau_D^{-1/2} + \frac{\gamma}{\tau_D}\right\} - i_P = 0 \quad (52)$$

Where we have set:

$$\alpha = 0.446 \frac{(nF)^{3/2}}{(RT)^{1/2}} A\Gamma \upsilon^{1/2}$$
$$\beta = 0.56\sqrt{\frac{nF\upsilon}{RT}} \quad (53)$$
$$\gamma = 0.05\left(\frac{nF\upsilon}{RT}\right)$$

The roots τ_D of the non-linear expression $G(\tau_D) = 0$ can be obtained from a standard numerical protocol such as the Bisection algorithm [59]. Hence the diffusive frequency $\tau_D = D/L^2$ can be evaluated provided the peak current i_P and surface coverage Γ are known at a particular sweep rate υ. Furthermore if the layer thickness L can be estimated then the diffusion coefficient D can be evaluated.

We have used both eqn.52 and a Randles-Sevcik analysis to numerically evaluate the diffusive frequency $\tau_D = D/L^2$. The results are compared graphically in fig.27 for a series of multi-cycled Ni electrodes. We see that similar results are obtained using the two procedures. The diffusive frequency decreases smoothly with increasing number of oxide growth cycles N.

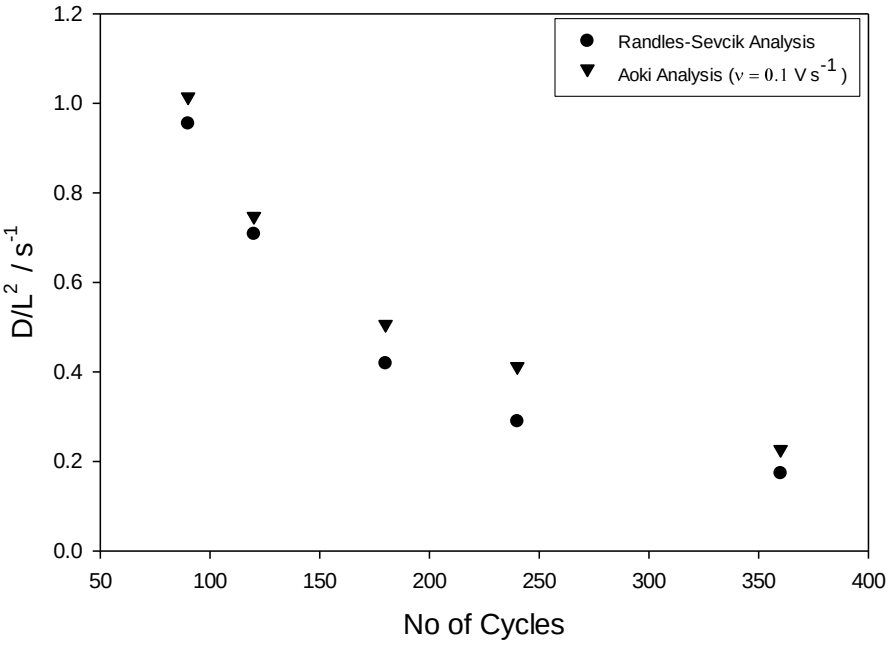

Figure 27. Variation of diffusive frequency characterizing redox switching in multicycled hydrous oxide coated Ni electrodes in 1.0 M NaOH with number of oxide growth cycles.

Finally Aoki [50] has also developed an expr4ession which relates the normalised peak width at half peak height to the parameter $\sqrt{W}$. The relevant expression is presented below:

$$\Delta\vartheta_{1/2} = \frac{nF}{RT}\Delta E_{p/2} = 5.72 + 2.20\tanh[Z] \qquad (54)$$

Where

$$Z = 1.38\psi + 0.40\psi^3 \qquad (55)$$

And

$$\psi = W^{0.30} - 1.96 \qquad (56)$$

Eqn.54 is plotted in fig.28 again using SigmaPlot. We note that for W = 0, $\Delta\vartheta_{1/2} = 3.5$ and $\Delta E_{p/2} = 3.5\frac{RT}{nF} = \frac{0.089}{n}V$ for n = 1 at T = 298 K. This is the limiting result for a surface wave as previously noted. For W = 50 we can show that $\Delta\vartheta_{1/2} = 7.8951$ and $\Delta E_{p/2} = 0.202V$.

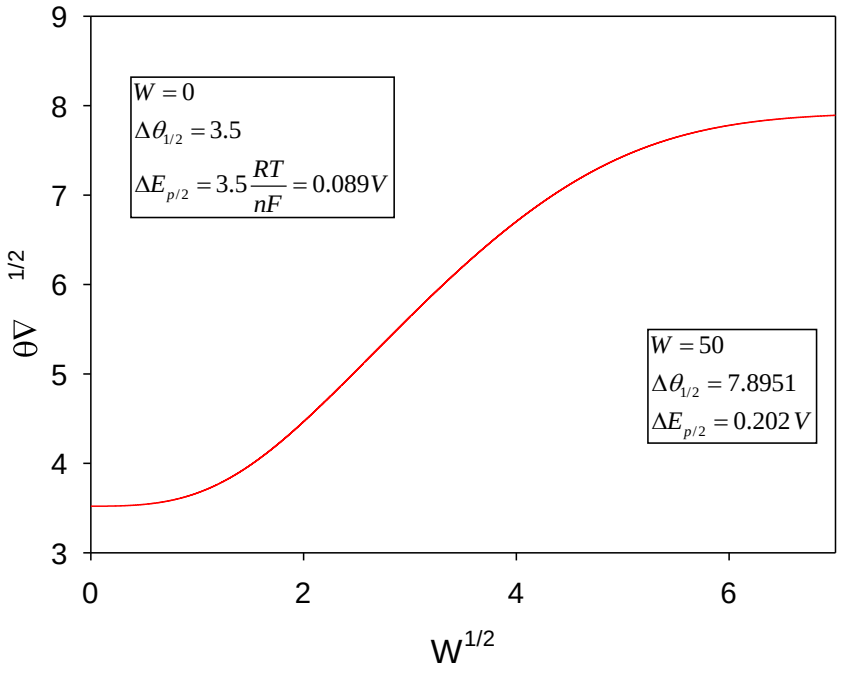

Figure 28. Variation of normalised voltammetric peak width at half peak height according to the Aoki Model. Curve calculated via eqn.54.

In principle it is also possible to use peak width data to evaluate the diffusive time constant but we have chosen not to adopt this approach. We conclude that the Aoki analysis (bearing its

intrinsic limitations in mind) provides a very useful approximate model to obtain quantitative redox switching information form perusal of cyclic voltammetry data as a function of sweep rate. We also have not estimated the layer thickness L in order to compute a charge transfer diffusion coefficient given the approximations and uncertainties inherent in layer thickness estimation. Instead we are content to deal with the diffusive frequency given by $\tau_D = D/L^2$.

3.3 Oxygen evolution electrocatalytic studies

In this section we describe the results of a comprehensive kinetic analysis carried out at hydrous oxide coated Ni electrodes in aqueous alkaline solution. These studies were performed both as a function of base concentration and hydrous oxide layer thickness. These studies follow on from a recently published paper in this journal [60] which describes enhanced oxygen evolution at hydrous oxy-hydroxide modified iron electrodes in aqueous alkaline solution. We also refer to an earlier paper written by Lyons and Brandon [61] which describes the OER mechanism and kinetics at oxidized (but not potential multicycled) Ni electrodes in base.

Typical steady state polarization curves for the OER recorded at a series of multicycled Ni electrodes in 1.0 M NaOH solutions are outlined in fig. 29. It is clear from these plots that the slope of the linear Tafel region located between 0.6 V and 0.7 V remains invariant with oxide charge capacity (the latter being related to the number of oxide growth cycles). Furthermore the current recorded at a given potential increases with increasing oxide charge capacity and the potential recorded at a fixed current decreases with increasing oxide charge capacity.

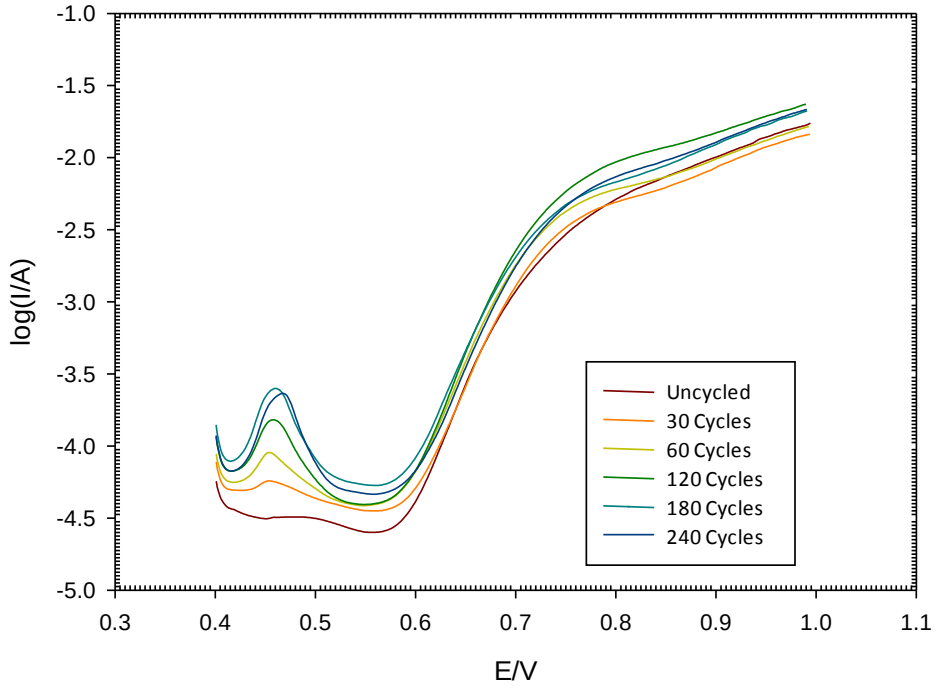

Figure 29. Typical steady state polarization curves (iR corrected) for active oxygen evolution at a series of multicycled Ni electrodes in 1.0 M NaOH solution at 298 K.

These points are further outlined in fig. 30 presented below where the variation with oxygen evolution rate (measured at a number of fixed overpotentials in the linear Tafel region) with average hydrous oxide charge capacity is presented.

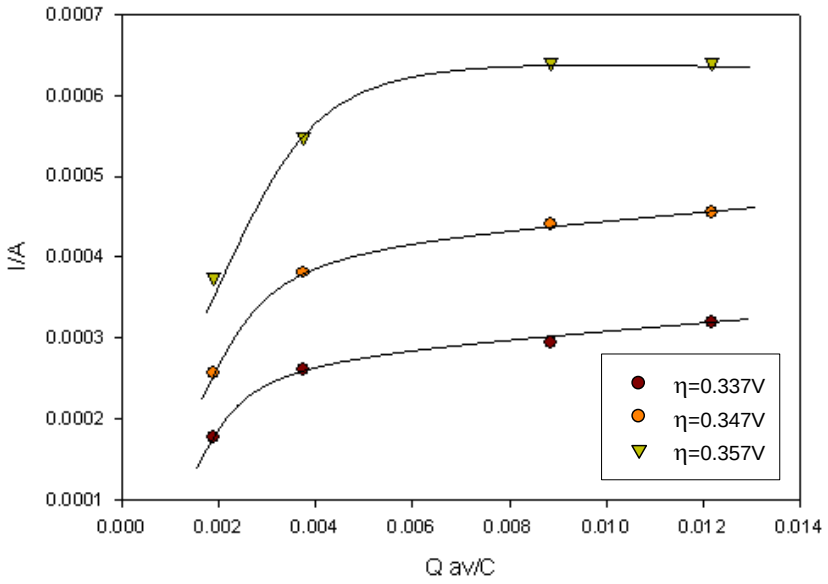

Figure 30. Variation of OER current recorded at a series of fixed over-potentials in the linear Tafel region as a function of average oxide charge capacity Q. Tafel plots were recorded in 1.0 M NaOH.

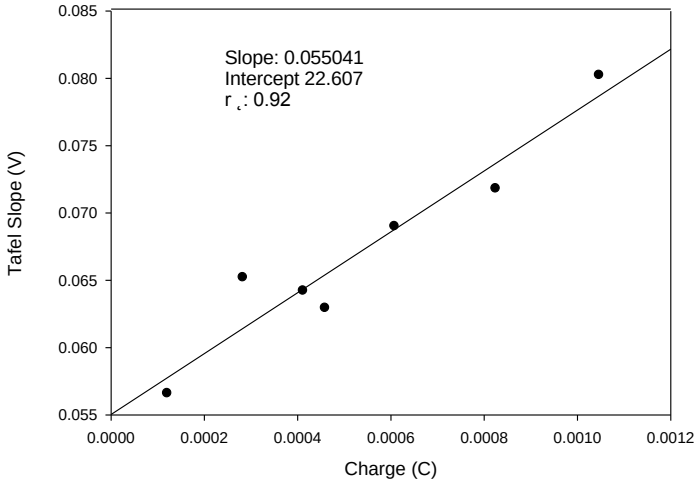

Figure 31. Variation of OER Tafel slopes recorded at low overpotentials with hydrous oxide charge capacity value Q. Tafel plots were recorded in 1.0 M NaOH.

Tafel slopes (measured in 1.0 M NaOH) were found to vary between 55 – 80 mV dec^{-1} over the range of oxide charge capacities examined. Typically as illustrated in fig.31, the Tafel slope recorded at low potentials increases in a regular manner with increasing oxide charge capacity

from a low of ca. 57 mVdec^{-1} to a high of ca. 80 mVdec^{-1}.

Typical steady state Tafel plots were also recorded as a function of base concentration over an extended range of the latter. The results for a thin film (N = 30 oxide growth cycles) are presented in fig.32 and those for a somewhat thicker layer (N = 120 cycles) are illustrated in fig. 33. In both cases Tafel slopes close to ca. 60 mV dec^{-1} are noted at low potentials and close to ca. 120 mV dec^{-1} at higher potentials.

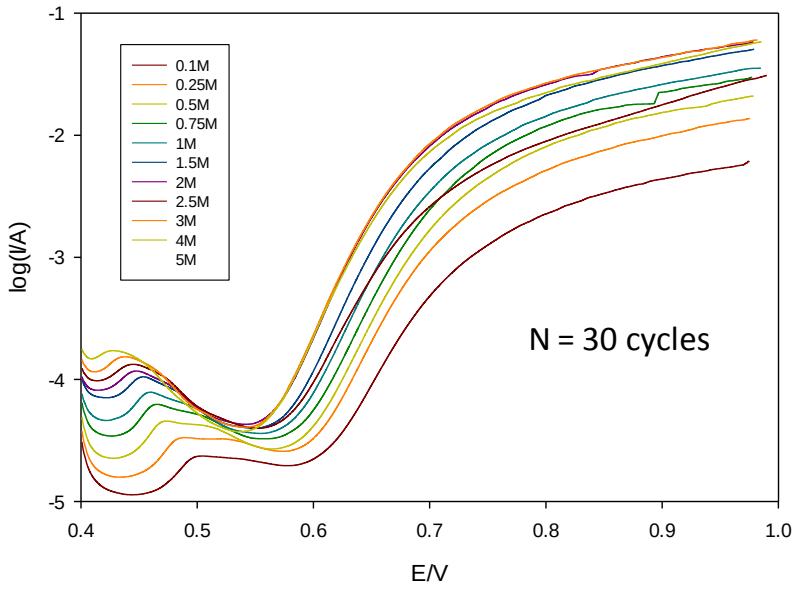

Figure 32. Typical Tafel plots for active oxygen evolution recorded for a hydrous oxide coated Ni electrode (N = 30 growth cycles in 1.0 M NaOH) as a function of base concentration.

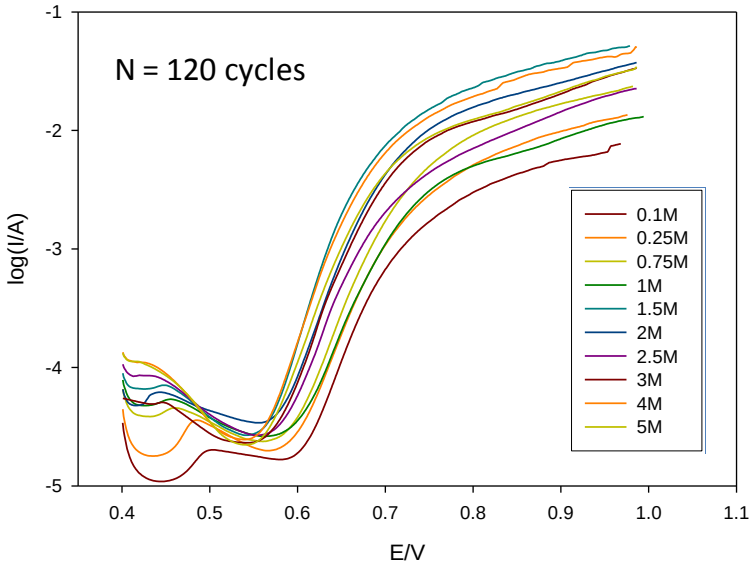

Figure 33. Typical Tafel plots for active oxygen evolution recorded for a hydrous oxide coated Ni electrode (N = 120 growth cycles in 1.0 M NaOH) as a function of base concentration.

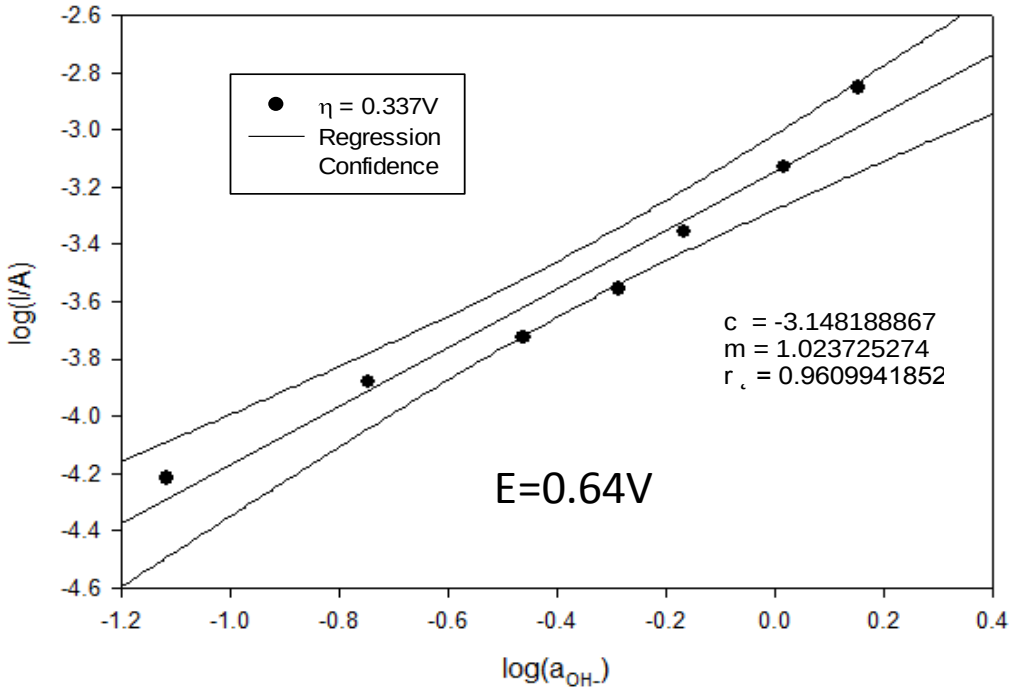

Figure 33. Typical Reaction order with respect to Oxygen evolution recorded for a thin hydrous oxide coated Ni electrode (N = 30 oxide growth cycles, 1.0 M NaOH) in the low Tafel slope region (E = 0.64 V or η = 0.337 V).

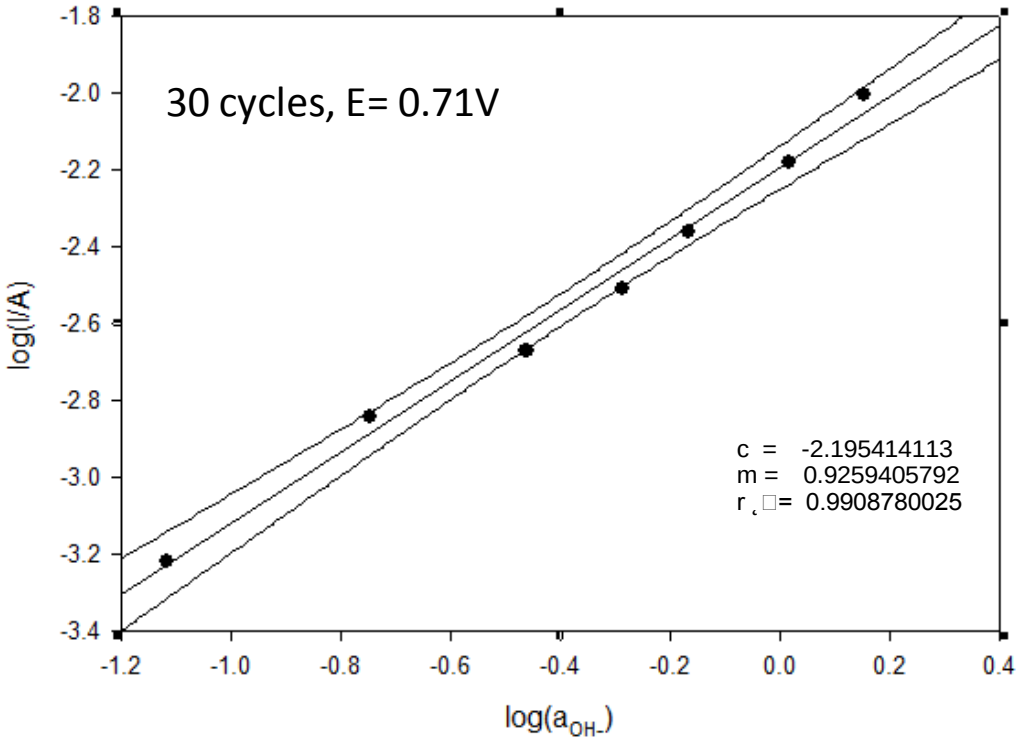

Figure 34. Typical Reaction order with respect to Oxygen evolution recorded for a thin hydrous oxide coated Ni electrode (N = 30 oxide growth cycles, 1.0 M NaOH) in the high Tafel slope region (E = 0.71 V or η = 0.407 V).

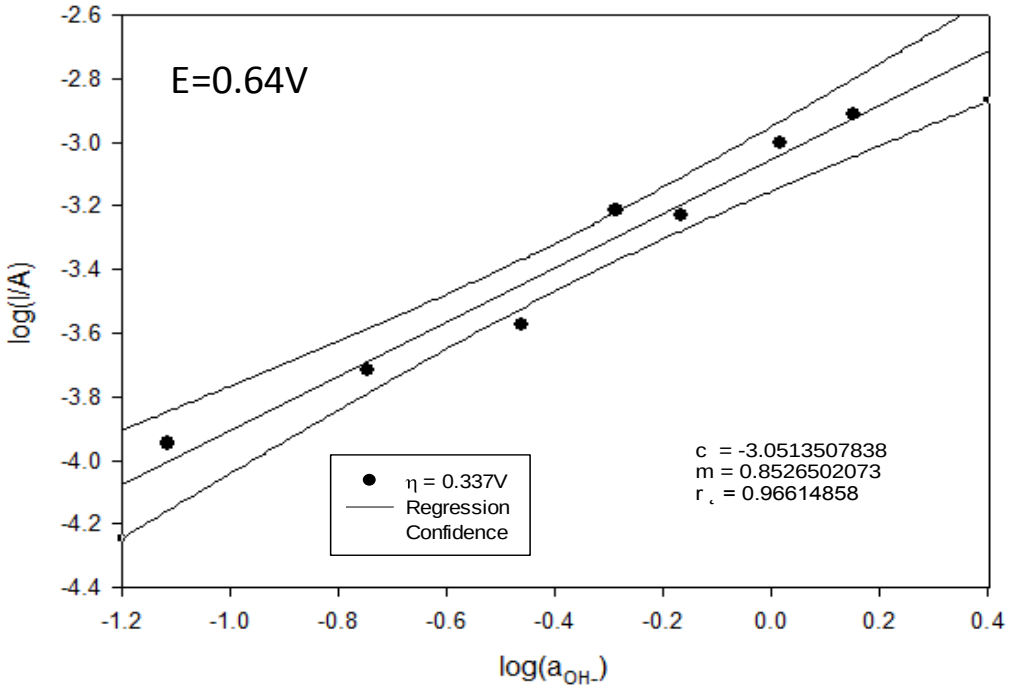

Figure 35. Typical Reaction order with respect to Oxygen evolution recorded for a thin hydrous oxide coated Ni electrode (N = 120 oxide growth cycles, 1.0 M NaOH) in the low Tafel slope region (E = 0.64 V or η = 0.337 V).

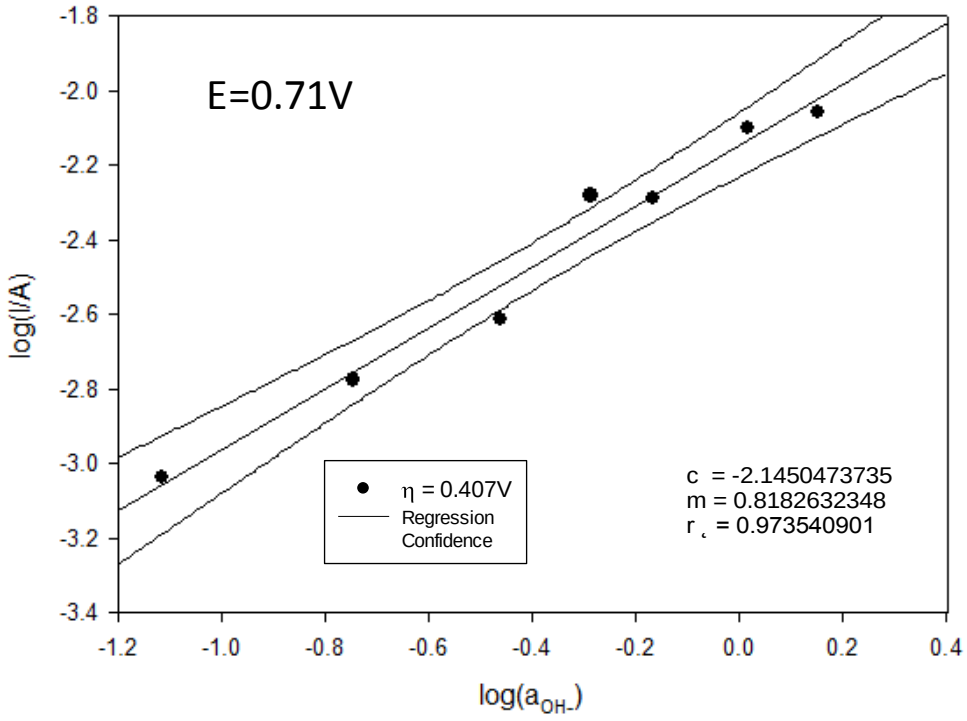

Figure 36. Typical Reaction order with respect to Oxygen evolution recorded for a thin hydrous oxide coated Ni electrode (N = 120 oxide growth cycles, 1.0 M NaOH) in the high Tafel slope region (E = 0.71 V or η = 0.407 V).

A series of reaction order studies were performed both in the low and high Tafel slope regions for thin and thicker hydrous oxide layers. The results are presented in fig.33-36 below. For the thinner oxide films the reaction orders were $m_{OH^-} = \left(\frac{d \log i}{d \log a_{OH^-}} \right) = 1.02$ in the low Tafel slope region and $m_{OH^-} = 0.93$ in the high Tafel slope region. The corresponding values recorded for thicker films were $m_{OH^-} = 0.85$ and $m_{OH^-} = 0.82$ in the low and high Tafel slope regions respectively.

Hence any mechanism must rationalise a dual Tafel slope behaviour and a constant reaction order with respect to OH^- ion activity of unity irrespective of overpotential. In summary, a kinetic analysis and associated reaction mechanism for the OER at both the uncycled and multicycled Ni electrodes considered in this article, must predict that $b = 2.303 \times RT/F$ and the reaction order $m_{OH^-} = 1.0$ at low potentials, changing to $b = 2.303 \times 2RT/F$ and $m_{OH^-} = 1$ at higher potentials.

A plausible mechanism to account for the reported kinetic data for the OER at multicycled Ni electrodes in aqueous base can be outlined as follows.

$$[MO_m(OH)_n(OH_2)_y]^{p-} + OH^- \rightarrow [MO_m(OH)_n(OH^*)(OH_2)_{y-1}]^{p-} + H_2O + e^- \quad (57)$$

$$[MO_m(OH)_n(OH^*)(OH_2)_{y-1}]^{p-} \rightarrow [MO_m(OH)_{n+1}(OH_2)_{y-1}]^{p-} \quad (58)$$

$$[MO_m(OH)_{n+1}(OH_2)_{y-1}]^{p-} \rightarrow [MO_m(OH)_{n+1}(OH_2)_{y-1}]^{(p-1)-} + e^- \quad (59)$$

$$[MO_m(OH)_{n+1}(OH_2)_{y-1}]^{(p-1)-} + 2OH^- \rightarrow [MO_m(OH)_{n-1}(OH_2)_{y-1}]^{(p-1)-} + O_2 + 2H_2O + 2e^- \quad (60)$$

$$[MO_m(OH)_{n-1}(OH_2)_{y-1}]^{(p-1)-} + OH^- + H_2O \rightarrow [MO_m(OH)_n(OH_2)_y]^{p-} \quad (61)$$

This mechanism involves the invocation of a Ni(III) oxidation state throughout and does not suggest the formation of a Ni(IV) state. We represent the mechanistic sequence in terms of linked networked octahedral surfaquo groups in an extended microdisperse open polymeric framework in which the central metal ion (M = Ni(III)) is coordinated to hydroxyl (OH), oxide (O) and water (OH_2) ligands. We note that $p = 2m + n - 3$. The second non-eletrochemical step (eqn.58) in the reaction sequence is rate determining at low overpotentials and the initial discharge step (eqn.57) becomes rate limiting at high overpotentials. The latter expression involves the relaxation of a coordinated OH ligand between two energetically inequivalent positions (labelled OH* and OH).

Specifically we can outline the following mechanism which is similar to that recently outlined by us for hydrous oxide coated Fe electrodes in aqueous base [8,10,52]:

$$[Ni(III)O_m(OH)_n]^{p-} + OH^- \rightarrow [Ni(III)O_m(OH)_n(OH^*)]^{p-} + e^- \quad (62)$$

$$[Ni(III)O_m(OH)_n(OH^*)]^{p-} \rightarrow [Ni(III)O_m(OH)_{n+1}]^{p-} \quad (63)$$

$$[Ni(III)O_m(OH)_{n+1}]^{p-} \rightarrow [Ni(III)O_m(OH)_{n-1}]^{(p-1)-} - - H_2O_2 + e^- \quad (64)$$

$$[Ni(III)O_m(OH)_{n-1}]^{(p-1)-} - - H_2O_2 + 2OH^- \rightarrow [Ni(III)O_m(OH)_n]^{p-} - - HO_2 + H_2O + e^- \quad (65)$$

$$[Ni(III)O_m(OH)_n]^{p-} - - HO_2 + OH^- \rightarrow [Ni(III)O_m(OH)_n]^{p-} + O_2 + H_2O + e^- \quad (66)$$

Again we note that $p = 2m + n - 3$, and the rate limiting second step again involves a structural rearrangement of an energetically in-equivalent coordinated hydroxyl ligand. Following Bockris and Otagawa [62], we also invoke the formation of a physisorbed peroxide entity S—H_2O_2. Note that in the step presented in eqn.64 the electron lost to the external circuit is provided by an excess co-ordinated OH^- ion, leading to an overall decrease of one unit in the net negative charge of the surface complex. The suggestion that the OER mechanism involves a NI(III) hydroperoxy intermediate of the form S—HO_2^- is attractive and has received some experimental backing from recent spectroscopic measurements [63]. In the scheme outlined in eqn.62-eqn. 66 above the catalytically active intermediate species are represented as complex anionic entities, in agreement with the observed acid/base properties of the hydrated oxide film. We believe that this approach is more realistic than thinking in terms of discrete simple stoichiometric oxy-hydroxide species.

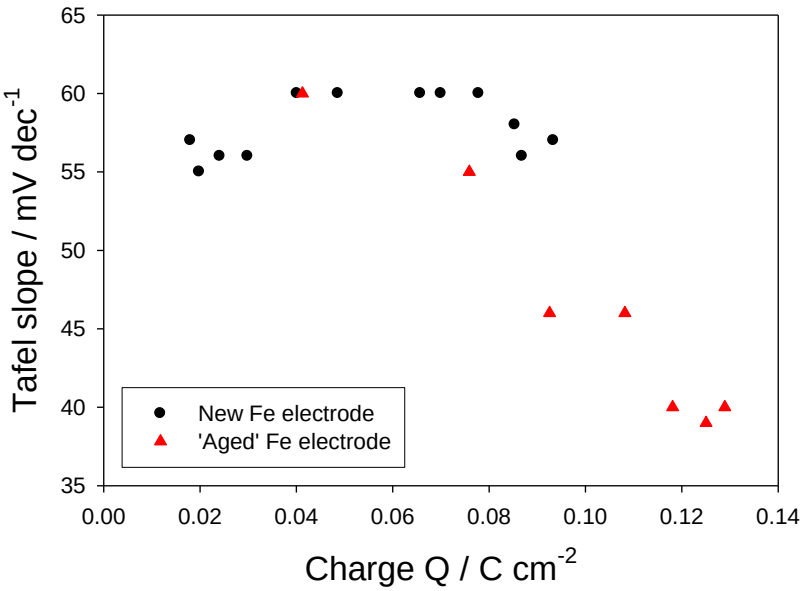

Figure 37. Variation of steady state Tafel slope values recorded at low potentials in OER region as a function of oxide redox charge capacity. Curves recorded for multicycled Fe electrodes in 1.0 M NaOH.

The observation that the Tafel slope observed at low overpotentials increases with increasing hydrous oxide charge capacity is directly at variance with similar experiments performed with

multicycled iron oxide electrodes in aqueous base solution [52]. In the latter case the gradual lowering in Tafel slope with increasing charge capacity value (outlined in fig.37) indicates that electro-catalytic efficiency increases with increasing hydrous oxide film thickness (expressed as redox charge capacity Q). We agree with the analysis proposed by Burke and O'Sullivan [64,65] that the gradual lowering of the low Tafel slope value from ca. 55 $mVdec^{-1}$ to ca. 40 $mVdec^{-1}$ with increase in hydrous oxide charge capacity Q could well suggest that hydrated oxide formation occurs initially by an 'island' mechanism- the lower slope being reached when the metal surface is completely covered with hydrous oxide. Alternatively, and this is more probable, the change could well be due to a gradual increase in the extent of hydration of a film of uniform thickness, at low values of the latter, with increasing charge storage capacity. The data observed in fig.31 for multicycled Ni electrodes in aqueous base could then be rationalized by assuming that the oxide layer becomes less hydrated with increasing number of potential cycles. The higher slopes (ca. 80 $mVdec^{-1}$ compared with ca. 55 $mVdec^{-1}$) observed for nickel oxide electrodes of higher charge capacity could then suggest the operation of weaker hydroxyl coordination of the intermediates at the relatively anhydrous oxide on this surface, so that the rate of oxygen evolution is not determined exclusively by interactions between the intermediates, as seems to be the case on the more hydrated layers. Hence the initial fast OH^- ion discharge may have a greater influence on the kinetics of the overall OER process in the case of these thicker less hydrated films. The opposite pertains to thick iron oxide films [52].

The increase in OER current (recorded at fixed driving force or overpotential) with increasing oxide redox charge capacity as outlined in fig. 30 is not to be unexpected since the real surface area of the oxide is increasing and consequently the number of catalytically active surfaquo groups available to participate in the oxygen evolution process is also increasing. We will note in section 3.3 that the oxygen evolution rate is directly proportional to Γ_S the surface concentration of Ni(III) surfaquo groups (at least for low values of the redox charge capacity), and so the data outlined in fig. 31 is not surprising.

Other mechanistic approaches can be suggested. For instance the pathway of O'Grady and Yeager [66], originally formulated to explain OER polarization data obtained on RuO_2 electrodes in alkaline solution is presented below:

$$S^z + OH^- \rightarrow (SOH)^z + e^- \quad (67)$$

$$(SOH)^z \rightarrow (SOH)^{z+1} + e^- \quad (68)$$

$$2(SOH)^{z+1} + 2OH^- \rightarrow 2S^z + O_2(g) + 2H_2O \quad (69)$$

In this pathway, z is the oxidation state of the metal ion of the electrocatalytically active surface site S. The suggestion is that a complex species $(SOH)^z$ is formed by the initial discharge of an OH^- ion at a metal ion site S^z- this electron is transferred directly to the external circuit, with the oxidation state of the central metal ion of the surfaquo group remaining umchanged. In the second step this surfaquo metal ion is oxidized from S^z to S^{z+1} with transfer of a further electron

without discharge of a second OH^- ion. In publications from this group on the OER at RuO_2 [67, 68] and by Burke and O'Sullivan on the OER at oxidized Rh [65], the first two steps of the pathway can be generally represented as:

$$(S(z))^{p-} + OH^- \rightarrow (S(z+1)OH)^{p-} + e^- \qquad (70)$$

$$(S(z+1)OH)^{p-} \rightarrow (S(z+1)OH)^{(p-1)-} + e^- \qquad (71)$$

where, $(S(z))^{p-}$ represents a complex hydrous oxide catalytic site with a central metal ion in the + z oxidation state- p is a positive integer. It is noteworthy, that in contrast to the pathway proposed by O'Grady and Yeager, oxidation of the central metal ion occurs in the initial discharge step presented in eqn.70, with the second electron transfer ocuring to a one electron discharge of the overall charge on the complex surface species. The logic of the O'Grady-Yeager or the Lyons-Burke-O'Sullivan mechanisms is that oxygen evolution occurs to effectively 'quench' an unstable higher oxide moeity. We can utilize this concept to propose a mechanism for the OER at oxidized Ni electrodes in aqueous base.

We recall from our earlier discussion regarding the complex electrochemistry of the oxidation of Ni(II) species to higher oxidation states, that the highest whole number oxidation state in Ni(III). In any case this is the valence state for b-NiOOH, allegedly the 'right type of oxide' for the OER [3]. In consideration of this idea we believe that another feasible pathway for the OER at Ni in base involves the generation of a NI(IV) intermediate according to the following reaction sequence:

$$\left[Ni(III)O_m(OH)_n\right]^{p-} + OH^- \rightarrow \left[Ni(IV)O_m(OH^*)(OH)_n\right]^{p-} + e^- \qquad (72)$$

$$\left[Ni(IV)O_m(OH)_n OH^*\right]^{p-} \rightarrow [Ni(IV)O_m(OH)_{n+1}]^{p-} \qquad (73)$$

$$[Ni(IV)O_m(OH)_{n+1}]^{p-} \rightarrow [NI(IV)O_m(OH)_{n+1}]^{(p-1)-} + e^- \qquad (74)$$

$$[Ni(IV)O_m(OH)_{n+1}]^{(p-1)-} + 2OH^- \rightarrow [Ni(III)O_m(OH)_{n-1}]^{(p-1)-} + O_2(g) + 2H_2O + e^- \qquad (75)$$

$$[Ni(III)O_m(OH)_{n-1}]^{(p-1)-} + OH^- \rightarrow [Ni(III)O_m(OH)_n]^{p-} + e^- \qquad (76)$$

It is clear that the mechanism presented in eqn.62-66 or that presented in eqn.72-eqn.76 both can account for the kinetic data presented in this paper. The nature of the hydrated surface species such as $[Ni(III)O_m(OH)_n]^{p-}$ where $p = 2m + n - 3$ is in keeping with the anionic character of hydrous oxides. It is quite likely that m = 1 and so the latter species is merely a NiOOH surface group that has coordinated extra hydroxide ions owing to the acidic nature of the hydrous oxide.

Although our electrochemical measurements have lead to the suggestion of two candidate mechanisms, these measurements cannot further discriminate between the two. The Ni(IV)

intermediate mechanism outlined in eqn.72-eqn.76 will appeal to those that envisage the OER to be essentially a 'side reaction' facilitating the decomposition of unstable oxide moieties. In contrast one of the major advantages of the Ni(III) intermediate mechanism is that it can account satisfactorily for the observed loss of oxygen evolution activity with time that was observed by Liu and Srinivasan [3]. Quite reasonably, these authors attributed this behaviour to an increase in the relative proportion of Ni^{4+} compared with Ni^{3+} surface ions, envisaged to occur by the oxidation, upon extended polarization, of the catalytically active β-NiOOH to NiO_2. However, their proposed mechanism (a modified Krasil'shchikov scheme [69]) also proposed that NiO_2 partakes in the OER as a transient reaction intermediate. It is rather difficult however to rationalise how the Ni(IV) species can present an inert surface site for the OER, yet act as an intermediate for the same reaction. This difficulty is removed by our pathway outlined in eqn.62-eqn.66 which only involves a Ni(III) intermediate. The latter pathway is also consistent with an OER mechanism recently proposed by our group for hydrous iron oxide layers.The latter scheme involves an Fe(VI) hydroperoxy intermediate, and is outlined below. Here, the catalytically active and intermediate species are represented as complex anionic entities, where, in the present case p=2m+n-6. We believe that this approach is more realistic than thinking in terms of discrete simple stoichiometric oxy-hydroxide species.

$$[Fe(VI)O_m(OH)_n]^{p-} + OH^- \rightarrow [Fe(VI)O_{m+1}(OH)_{n-1}]^{p-} + H_2O + e^- \quad (77)$$

$$[Fe(VI)O_{m+1}(OH)_{n-1}]^{p-} + OH^- \rightarrow [Fe(VI)O_m \underline{OOH}(OH)_{n-1}]^{p-} + e^- \ldots RDS \quad (78)$$

$$[Fe(VI)O_m \underline{OOH}(OH)_{n-1}]^{p-} + OH^- \rightarrow [Fe(VI)O_m \underline{OO}(OH)_{n-1}]^{p-} + H_2O + e^- \quad (79)$$

$$[Fe(VI)O_m \underline{OO}(OH)_{n-1}]^{p-} + OH^- \rightarrow [Fe(VI)O_m(OH)_n]^{p-} + O_2 + e^- \quad (80)$$

We have previously noted that the oxide film produced by the potential multi-cycling of an Fe electrode will be significantly more hydrated than that obtained by the passivation of relatively un-aged Fe surfaces. The amount of amphoteric character displayed by an anodic oxide is expected to be proportional to its degree of hydration. It is therefore expected that "aged" and multi-cycled Fe electrodes would contain a larger surface density of the catalytically active, complex anionic $[Fe(VI)O_m(OH)_n]^{p-}$ species at lower overpotentials, relative to fresher Fe electrodes. Note that the concept of the catalytically active site existing in the form of an hydroxylated anionic surface complex is maintained – for Fe(VI), p = 2m+n-6. Indeed, since Fe(VI) species (probably in the form of FeO_4^{2-}) are soluble in aqueous alkaline solution , their stabilization on the oxide surface by the coordination of excess OH^- ions provides a tentative explanation as to how they can act as OER active centers. Lyons and Brandon [10,52, 60] noted that the OER pathway defined in eqn. 77 – eqn. 80 above is also suitable for Co anodes, except in this case the active site is represented as $[Co(IV)O_m(OH)_n]^{p-}$ (p = 2m+n-4), in agreement with the proposal of Gennero De Chialvo et al. [70,71] that the catalytic species is likely to exist as discrete CoO_2 entities.

3.3 Steady state kinetic analysis of multi-cycled Ni electrodes in aqueous base

We now proceed with a kinetic analysis of the mechanism presented generally in eqn.62 – eqn.66 and assume that at lower overpotentials there prevails a *low* coverage of S-OH species. Therefore a *Langmuir adsorption isotherm* is applicable .

At low values of overpotential, the chemical rearrangement step outlined in eqn.63 is rate determining and we may write that the net flux (unit: molcm^{-2}s^{-1}) is given by:

$$f_{\Sigma} = k_2' \Gamma_{SOH*} \tag{81}$$

Where we note that Γ_{SOH*} represents the surface concentration (units: mol cm^{-2}) of the anionic complex $[Ni(III)O_m(OH)_n OH*]^{p-}$, and $k_2' = k_2^0$ (unit: s^{-1}) is the potential independent heterogeneous rate constant for the hydroxyl rearrangement reaction outlined in eqn.63. We now use the quasi steady state analysis to evaluate the surface concentration of the Ni(III) intermediate, and write that:

$$\frac{d\Gamma_{SOH*}}{dt} = k_1' \Gamma_S a_{OH^-} - k_{-1}' \Gamma_{SOH*} - k_2^0 \Gamma_{SOH*} \cong 0 \tag{82}$$

Hence we find:

$$\Gamma_{SOH*} \cong \frac{k_1' \Gamma_S a_{OH^-}}{k_{-1}' + k_2^0} = \frac{k_1^0 \Gamma_S a_{OH^-} \exp\left[\dfrac{\beta F \eta}{RT}\right]}{k_{-1}^0 \exp\left[-\dfrac{(1-\beta) F \eta}{RT}\right] + k_2^0} \tag{83}$$

Hence the net flux is given by:

$$f_{\Sigma} = \frac{i}{4FA} = \frac{k_1^0 k_2 \Gamma_S a_{OH^-} \exp\left[\dfrac{\beta F \eta}{RT}\right]}{k_{-1}^0 \exp\left[-\dfrac{(1-\beta) F \eta}{RT}\right] + k_2^0} \tag{84}$$

In the latter expressions we have assumed that the heterogeneous electrochemical rate constants associated with the initial reaction step are well described in terms of the Butler-Volmer equation and that β and η denote the symmetry factor ($0 \le \beta \le 1$) and overpotential respectively. Furthermore Γ_S denotes the surface concentration of the anionic Ni(III) surfaquo complex $[Ni(III)O_m(OH)_n]^{p-}$.

We assume that at low overpotentials the chemical step outlined in eqn.63 is rate limiting and so $k_2^0 << k_{-1}^0$ and hence eqn.84 reduces to:

$$f_{\Sigma} \cong k_2^0 \left(\frac{k_1^0}{k_{-1}^0} \right) a_{OH^-} \Gamma_S \exp\left[\frac{F\eta}{RT} \right] \qquad (85)$$

Hence we can readily show that the Tafel slope and reaction order with respect to hydroxyl ion activity are given by:

$$\begin{aligned} b &\cong 2.303\left(\frac{RT}{F} \right) \cong 60 \text{ mVdec}^{-1} \\ m_{OH^-} &= \left(\frac{d \log i}{d \log a_{OH^-}} \right) \cong 1.0 \end{aligned} \qquad (86)$$

In contrast, at higher overpotentials the initial discharge step outlined in eqn.62 is rate determining and so $k_2^0 >> k_{-1}^0$, and we can write:

$$f_{\Sigma} = \frac{i}{4FA} \cong k_1^0 \Gamma_S a_{OH^-} \exp\left[\frac{\beta F\eta}{RT} \right] \qquad (87)$$

And the Tafel slope and reaction order with respect to hydroxide ion activity is predicted to be:

$$\begin{aligned} b &\cong 2.303\left(\frac{2RT}{F} \right) \cong 120 \text{ mVdec}^{-1} \\ m_{OH^-} &\cong 1.0 \end{aligned} \qquad (88)$$

The latter diagnostic parameters (obtained by assuming that $\beta \cong 0.5$) are in excellent agreement with those experimentally obtained. Hence the OER kinetics can be rationalised using a relatively simple mechanistic analysis.

4. CONCLUSIONS

We now summarise the principal conclusions arising from the present paper regarding the formation, redox properties and electrocatalytic activity with respect to the OER of hydrous oxide coated Ni electrodes in aqueous alkaline solution. First, hydrous microdispersed oxides are readily prepared via the repetitive cyclic potential sweep method applied to the parent metal in aqueous alkaline solution. The latter method is very similar to that employed in the electropolymerization of Electronically Conducting Polymer (ECP) films such as poly(pyrrole) or poly(aniline). The oxide/solution interface has a duplex character, consisting of an inner, largely anhydrous compact oxide, and an outer, hydrated microdisperse oxide layer which exhibits significant electrocatalytic activity with respect to anodic oxygen evolution. Second, the charge storage/charge percolation

properties of the hydrous oxide depend on electrochemical and environmental variables such as the lower and upper potential sweep limits, the potential sweep rate, the base concentration employed, the solution temperature, and the solution pH. Third, the acid/ base behaviour of anodically formed transition metal oxides is important when considering the mechanism of both redox switching and oxygen evolution. Furthermore, hydrous oxides are more difficult to reduce than less hydrated compact materials, and this may well have a significant implication for the catalysis of the cathodic ORR. Fourth, we have examined the redox switching kinetics at hydrated nickel oxide in some detail and utilized theoretical models originally developed to describe transport and kinetics in polymer modified electrodes, to probe the diffusion of protons/hydroxyl ions through the hydrated oxide matrix. A diffusive frequency corresponding to protonic diffusion through the oxide was extracted via this analysis. Fifth we have noted from analysis of potential step chronoamperometry experiments that the current transients recorded for oxidative and reductive redox switching of hydrous oxide coated Ni electrodes in aqueous base are complex in shape. Sixth, with respect to the catalysis of the anodic OER process, the sole pathway, that can account for the entire set of experimental parameters observed is the *physisorbed hydrogen peroxide mechanism*. The second step of this pathway, which involves the rearrangement of a S-OH chemical bond, is considered to be rate limiting. The different values of *b* and m_{OH^-} observed for the same electrode at different overpotentials, arise due to changes in the in rate determining step, in contrast to that observed for hydrated iron oxide films. In general it is important to understand that , giving consideration to the acidic nature of hydrated oxide surfaces at high pH, is extremely useful in understanding the OER at transition metal surfaces in aqueous alkaline media. Since in general, the catalytic centres for oxygen evolution reside on the surface of an oxide phase in contact with aqueous solution, the surface region of the oxide will inevitably become somewhat hydrated. In view of this, it is our belief that all workers in this area should consider the amphoteric nature of their oxide surfaces, regardless of how the oxide phase was prepared. It is, for example, to take the case of a Ni anode in alkaline solution, more realistic to represent the OER active site as $[Ni(III)O_m(OH)_n]^{p-}$ (where extra hydroxide ions have been coordinated from solution, owing to the acidic nature of the oxide in electrolytes of high pH), rather than the traditional practice of considering it to be a discrete NiOOH entity.

ACKNOWLEDGEMENT & DEDICATION

This paper is dedicated to the memory of Professor Laurence D Burke, late of the Department of Chemistry, University College, Cork, Ireland who has recently passed away. Professor Burke was a first rate scientist and an excellent mentor and friend to many. The field of Physical Electrochemistry is much the poorer for his absence. He will be sorely missed.

This publication has emanated in part from research conducted with the financial support of Science Foundation Ireland (SFI) under Grant Number SFI/10/IN.1/I2969.

References

1. (a) D.E. Hall, *J. Electrochem. Soc.*, 130 (1983) 317.(b) K. Zeng and D. Zhang, *Prog. Energy Combust. Sci.*, 36 (2010) 307.(c) H. Tributsch, *Int. J. Hydrogen Energy*, 33 (2008) 5911.(d) G. W. Crabtree, M. S. Dresselhaus and M. V. Buchanan, *Phys. Today*, December 2004, 39.

2. K. Kinoshita, *Electrochemical Oxygen Technology*, Wiley-Interscience, New York,1992, chapter 2, pp. 78-99.
3. P.W.T. Lu and S. Srinivasan, *J. Electrochem. Soc.*, 125(1978) 1416.
4. B.E. Conway and P.L. Bourgault, *Can. J. Chem.*, 37(1959) 292.
5. B.E. Conway and P.L. Bourgault, *Trans. Faraday Soc.*, 58(1962 593.
6. R.D. Armstrong, G.W.D. Briggs and E.A. Charles, *J. Appl. Electrochem.*, 18(1988) 21.
7. E.B. Castro, S.G. Real and L.F. Pinheiro Dick, *Int. J. Hydrogen Energy.* 29(2004) 255.
8. M. E. G. Lyons and M. P. Brandon, *Int. J. Electrochem. Sci.*, 3 (2008) 1386.
9. M. E. G. Lyons and M. P. Brandon, *Int. J. Electrochem. Sci.*, 3 (2008) 1425.
10. M. E. G. Lyons and M. P. Brandon, *Int. J. Electrochem. Sci.*, 3 (2008) 1463.
11. P. He, L.R. Faulkner, *Anal. Chem.,* 58 (1986) 517.
12. M.E.G. Lyons, L.D. Burke, *J. Electroanal. Chem.*, 170 (1984) 377.
13. L. D. Burke and M. E. G. Lyons, *J. Electroanal. Chem.*, 198 (1986) 347.
14. M.E.G. Lyons, M.P. Brandon, *Phys. Chem. Chem. Phys.*, 11 (2009) 2203.
15. L.D. Burke, M.E. Lyons, O.J. Murphy, *J. Electroanal. Chem.*, 132 (1982) 247.
16. L. D. Burke, M. I. Casey, V. J. Cunnane, O. J. Murphy and T. A. M. Twomey, *J. Electroanal. Chem.*, 189 (1985) 353.
17. P. He, L.R. Faulkner, *Anal. Chem.,* 58 (1986) 517.
18. S. Gottesfeld and S. Srinivasan, *J. Electroanal. Chem*, 86(1978) 89.
19. A. Seghiouer, J. Chevalet, A. Barhoun and F. Lantelme, *J. Electroanal. Chem*, 442(1998) 113.
20. J.F. Wolf, L-S. Yeh and A. Damjanovic, *Electrochim. Acta*, 26(1981) 409.
21. J.L. Weininger and M.W. Breiter, *J. Electrochem. Soc.*, 110(1963) 484.
22. L.D.Burke, D.P. Whelan, *J. Electroanal. Chem.*, 109 (1980) 385.
23. A.C. Chialvo, W.E. Triaca, A.J. Arvia, *J. Electroanal. Chem.,* 146 (1983) 93.
24. (a) L.D. Burke, T.A.M. Twomey. *J. Electroanal. Chem.,* 162 (1984) 101.(b) L.D. Burke, T.A.M. Twomey, *J. Electroanal. Chem.,* 167 (1984) 285.
25. W. Visscher, E. Barendrecht, *J. Appl. Electrochem.,* 10 (1980) 269.
26. L.M.M. de Souza, F.P. Kong, F.R. McLarnon, R.H. Muller, *Electrochim. Acta.,* 42 (1997) 1253.
27. R. Šimpraga, B.E. Conway, *J. Electroanal. Chem.,* 280 (1990) 341.
28. A.C. Makrides, *J. Electrochem. Soc.*, 113 (1966) 1158.
29. M.Okuyama, S. Haruyama, *Corros. Sci.,* 14 (1974) 1.
30. (a) J.O'M. Bockris, M. Genshaw, V. Brusic, *Symp. Faraday Soc.,* 4 (1970) 177. (b) J.O'M. Bockris, V. Brusic, H. Wroblowa, *Electrochim Acta*., 16(1971) 1859. (c) H. Wroblowa, V. Brusic, J.O'M. Bockris, *J. Phys. Chem*., 75 (1971) 2823.
31. L.M.M. de Souza, F.P. Kong, F.R. McLarnon, R.H. Muller, *Electrochim. Acta.,* 42 (1997) 1253.
32. S.D. James, *J. Electrochem. Soc.,* 116 (1969) 1681.
33. J.W. Schultze, K.H. Vetter, *Electrochim. Acta,* 18 (1973) 889.
34. W.M. Sachtler, L.L.V. Reizen, *J. Res. Inst. Catal., Hokkaido Univ.,* 10 (1962) 87.
35. R. Woods in *Electroanal. Chem*., Vol. 9, Ed. A.J. Bard, Marcel Dekker, New York, 1976, Ch. 1.
36. L.D.Burke, E.J.M. O'Sullivan, *J. Electroanal. Chem.,* 117 (1981) 155.
37. H. Bode, K.Dehmelt, J. Witte, *Electrochim. Acta.,* 11 (1966) 1079.
38. L.D. Burke, M.E.G. Lyons, *Mod. Asp. Electrochem*., 18 (1986) 169-248.
39. (a) L.D. Burke, M.E.G. Lyons, *J. Electroanal. Chem.,* 198 (1986) 347. (b) L.D. Burke, E.J.M. O'Sullivan, *J. Electroanal. Chem*., 93 (1978) 11.
40. L. D. Burke and D. P.Whelan, *J. Electroanal. Chem.,* 162 (1984) 121.
41. R.A. Robinson and R.H. Stokes, *Electrolyte Solutions*, Butterworths, London, 1965, p.492.
42. L.D.Burke, T.A.M. Twomey, *J. Electroanal. Chem.,* 134 (1982) 353.
43. (a) D.M. MacArthur, *J. Electrochem. Soc.,* 117 (1970) 422.(b) D.M. MacArthur, *J. Electrochem. Soc.*, 117 (1970) 729.
44. A.H. Zimmerman, P.K. Effa, *J. Electrochem. Soc.,* 129 (1984) 983.

45. (a) J.W. Weidner, P. Timmerman, *J. Electrochem. Soc.*, 141 (1994) 346. (b) S. Motupally, C.C. Streinz, J.W. Weidner, *J. Electrochem. Soc.*, 142 (1995) 1401.
46. Z. Mao, P. De Vidts, R.E. White, J. Newman, *J. Electrochem. Soc.*, 141 (1994) 54.
47. (a) See for example http://en.wikipedia.org/wiki/Theta_function Accessed 16/09/2011.(b) R.P. Buck, T.R. Berube, *J. Electroanal. Chem.*, 256 (1988) 239.
48. J. Spanier, K.B. Oldham, *An atlas of functions*, Hemisphere Publishing Corporation, New York, 1987, Chapter 41, pp.395-403.
49. S.Motupally, C.C. Streinz, J.W. Weidner, *J. Electrochem. Soc.*, 145 (1998) 29.
50. (a) K. Aoki, K. Tokuda, H. Matsuda, *J. Electroanal. Chem.*, 146 (1983) 417. (b) K. Aoki, K. Tokuda, H. Matsuda, *J. Electroanal. Chem.*, 160 (1984) 33.
51. V. Mirceski, Z. Tomovski, *J. Solid State Electrochem.*, 15 (2011) 197.
52. M.E.G. Lyons, R.L. Doyle, M.P. Brandon, *Phys. Chem. Chem. Phys.*, 13 (2011) 21530.
53. R.W. Murray in *Molecular Design of Electrode Surfaces*, Ed. R.W. Murray, Techniques of Chemistry Series, Wiley Interscience, New York, 1992, vol. 22, ch. 1, pp. 1-48.
54. (a) J.C. Jernigan, C.E.D. Chidsey, R.W. Murray, *J. Am. Chem. Soc.*, 107 (1985) 2824; (b) C.E.D. Chidsey, R.W. Murray, *J. Phys. Chem.*, 90 (1986) 1479; (c) E.F. Dalton, N.A. Surridge, J.C. Jernigan, K.O. Wilbourne, J.S. Facci, R.W. Murray, *Chem. Phys.*, 141 (1990) 143; (d) J.C. Jernigan, N.A. Surridge, M.E. Zvanut, M. Silver, R.W. Murray, *J. Phys. Chem.*, 93 (1989) 4620.
55. M.E.G. Lyons, *Electroactive Polymer Electrochemistry*, Plenum Press, New York, 1994, ch.2, pp.102-103.
56. (a) E. Laviron, *J. Electroanal. Chem.*, 52 (1974) 395; (b) E. Laviron, *J. Electroanal. Chem.*, 112 (1980) 1; (c) E. Laviron, L. Roullier, C. Degrand, *J. Electroanal. Chem.*, 112 (1980) 11; (d) E. Laviron, *J. Electroanal. Chem.*, 122 (1981) 37; (e) E. Laviron, L. Roullier, *J. Electroanal. Chem.*, 115 (1980) 65; (f) E. Laviron, *J. Electroanal. Chem.*, 101 (1979) 19.
57. R.S. Nicholson, I. Shain, *Anal. Chem.*, 36 (1964) 706.
58. (a) J.M. Saveant, *Electrochem. Acta.*, 12 (1967) 999; (b) R.S. Nicholson, I. Shain, *Anal. Chem.*, 37 (1965) 178; (c) W.H. Reinmuth, *Anal. Chem.*, 34 (1962) 1446.
59. W.H. Press, S.A. Teukolsky, W.T. Vetterling, B.P. Flannery, *Numerical Recepies*, 2nd Edition, Cambridge University Press, Cambridge, UK, 1993, Chap. 9, pp.343-346.
60. M.E.G.Lyons, R.L. Doyle, *Int.J. Electrochem., Sci.*, 6 (2011) 5710.
61. M.E.G. Lyons, M.P. Brandon, *Int. J. Electrochem. Sci.*, 3 (2008) 1386.
62. J.O'M. Bockris, T. Otagawa, *J. Phys. Chem.*, 87 (1983) 2960.
63. (a) B.S. Yeo, S.L. Klaus, P.N. Ross, R.A. Mathies, A.T. Bell, *Chem. Phys. Chem.*, 11 (2010) 1854; (b) B.S. Yeo, A.T. Bell, *J. Am. Chem. Soc.*, dx.doi.org/10.1021/ja200559j
64. E.J.M. O'Sullivan, L.D. Burke, *Proc. Symp. Electrocatalysis*, W.E. O'Grady, P.N. Ross, F.G. Will, Eds., Electrochem. Soc., Pennington, NJ, 1982, pp.209-223.
65. E.J.M. O'Sullivan, L.D. Burke, *J. Electrochem. Soc.*, 137 (1990) 466.
66. W.O'Grady, C. Iwakura, J. Huang, E. Yeager, in *Proceedings Symposium on Electrocatalysis*, M.W. Brieter, Ed., Electrochemical Society, Pennington, NJ, 1974, p.286.
67. M.E.G. Lyons , L.D. Burke, J. Chem. Soc. Faraday Trans. I, 83 (1987) 299.
68. M.E.G. Lyons, S. Floquet, *Phys. Chem. Chem. Phys.*, 13 (2011) 5314.
69. A.I. Krasil'shchikov, *Zh. Fiz. Khim.* 37 (1963) 531.
70. M.R. Gennero De Chialvo, A.C. Chialvo, *Electrochim. Acta*, 33 (1988) 825.
71. M.R. Gennero De Chialvo, A.C. Chialvo, *Electrochim. Acta*, 35 (1990) 437.